Supplementary Information

Pseudouridine Residues as Substrates for Serum Ribonucleases

CLAIR S. GUTIERREZ,^{1,2,3} BJARNE SILKENATH,^{1,2} VOLGA KOJASOY,^{1,2} JAROSLAW A. PICH,¹ DANIEL C. LIM,⁴ and RONALD T. RAINES^{1,3,5}

¹Department of Chemistry, Massachusetts Institute of Technology, Cambridge, Massachusetts 02139, USA

Corresponding author: rtraines@mit.edu

Table of Contents

1. General Information	
1.1. Abbreviations	S2
1.2. Chemical Reagents and Instrumentation	S2
1.3. Biological Reagents and Instrumentation	S2
2. Synthesis	S4
3. Heterologous Production and Purification of RNase 1	
3.1. SDS-PAGE and LC-MS of RNase 1	S14
3.2. Activity Validation of Commercial RNase A and Recombinant RNase 1	S14
4. Experimentally Derived Extinction Coefficients of UpA, ΨpA, and m¹ΨpA	S17
5. UV spectra of UpA, ΨpA, and m¹ΨpA	S17
6. Additional Kinetic Data for Catalysis of UpA, ΨpA , and $m^1 \Psi pA$ Cleavage	S19
7. Kinetic Data for Catalysis of UpA Cleavage at Different pHs	S20
8. Statistics for X-Ray Crystallography	S21
9. Decavanadates in Crystal Structures	S25
10. Computational Analyses	
10.1. Top-Ranked Docking Poses of Enzyme·Substrate Complexes	S26
10.2. Molecular Dynamics Simulations of RNase A·Substrate Complexes	S27
10.3. Molecular Dynamics Simulations of RNase 1·Substrate Complexes	S27
10.4. RMSD and RMSF Plots for Molecular Dynamics Simulations of RNase A and	
11. Kinetic Data for Non-Enzymatic UpA and m¹ΨpA Cleavage	S32
12. NMR Spectra	S34
42 Deferences	0.47

³Broad Institute of MIT and Harvard, Cambridge, Massachusetts 02143, USA

⁴Department of Biology, Massachusetts Institute of Technology, Cambridge, Massachusetts 02139, USA

⁵Koch Institute for Integrated Cancer Research at MIT, Cambridge, Massachusetts 02139, USA

²These authors contributed equally

1. General Information

1.1. Abbreviations

BCA bicinchoninic acid

CHES 2-(cyclohexylamino)ethanesulfonic acid

DCM dichloromethane
DEPC diethyl pyrocarbonate
DMF dimethylformamide

EDTA ethylenediaminetetraacetic acid

EtOAc ethyl acetate

FRET fluorescence resonance energy transfer IPTG isopropyl β-D-1-thiogalactopyranoside

LC liquid chromatography

 m^{1} ΨpA N^{1} -methylpseudouridylyl(3' \rightarrow 5')adenosine m^{1} Ψ>ν N^{1} -methylpseudouridine 2',3'-cyclic vanadate MALDI matrix-assisted laser desorption/ionization

MES 2-morpholinoethanesulfonic acid

MMGBSA molecular mechanics-generalized Born surface area

MS mass spectrometry
MWCO molecular weight cutoff
OVS oligo(vinylsulfonic acid)

PAGE polyacrylamide gel electrophoresis

poly(A) poly(adenylic acid)
QTOF quadrupole time-of-flight

ΨpA pseudouridylyl(3' \rightarrow 5')adenosine Ψ>v pseudouridine 2',3'-cyclic vanadate

RMSD root-mean-square deviation RMSF root-mean-square fluctuation

RNase A bovine pancreatic ribonuclease (EC 3.1.27.5)

RNase 1 human ribonuclease 1 (EC 3.1.27.5)

SDS sodium dodecyl sulfate

TB terrific broth

TBSCl *tert*-butyldimethylsilyl chloride

THF tetrahydrofuran

TIC total ion chromatogram

Tris tris(hydroxymethyl)aminomethane

UpA uridylyl($3'\rightarrow 5'$)adenosine U>v uridine 2',3'-cyclic vanadate

UV ultraviolet vis visible

1.2. Chemical Reagents and Instrumentation

All procedures were performed at ambient temperature (~22 °C) and pressure (~1.0 atm) unless indicated otherwise. All reactions were performed in a reaction vial fitted with TFE-silicone septa

under $N_2(g)$ using standard Schlenk-line techniques. Reactions carried out at low temperatures were cooled by cooling agents in a Dewar vessel (water–ice bath at 0 °C).

Commercial chemicals were of reagent grade or better from Sigma–Aldrich (St. Louis, MO) and were used without further purification unless indicated otherwise. In all reactions involving anhydrous solvents, glassware was either oven- or flame-dried. Reagent-grade dichloromethane (DCM) was dried over a column of alumina and removed from a dry still under an inert atmosphere. All reactions were magnetically stirred and monitored by liquid chromatography—mass spectrometry (LC–MS) and analytical thin-layer chromatography. Purification was done with flash column chromatography performed with silica gel, typically using an Isolera One system from Biotage (Uppsala, Sweden), unless indicated otherwise. The term "concentrated under reduced pressure" refers to the removal of solvents and other volatile materials using a Buchi rotary evaporator (model R-210) at water aspirator pressure (<20 torr) while maintaining the water-bath temperature below 40 °C.

¹H, ¹³C, and ³¹P NMR spectra for compound characterization were acquired with an Avance Neo 500 MHz spectrometer from Bruker (Billerica, MA) in the Department of Chemistry Instrumentation Facility (DCIF) at MIT. ¹H and ¹³C NMR spectra were referenced to residual solvent peaks in CDCl₃ (¹H, 7.26 ppm; ¹³C, 77.16 ppm) or D₂O (¹H, 4.79 ppm). ¹³C NMR spectra in D₂O were referenced externally to TMS (0 ppm). ³¹P NMR spectra were referenced externally to 85% v/v H₃PO₄ (0 ppm). Multiplicities are abbreviated as s (singlet), d (doublet), t (triplet), q (quartet), and m (multiplet).

³¹P NMR spectra for non-enzymatic cleavage kinetics were acquired with a two-channel Avance-III HD Nanobay 400 MHz spectrometer from Bruker equipped with a 5 mm N₂(l)-cooled Prodigy cryoprobe.

Mass spectrometry was performed with an LCT electrospray ionization (ESI) 1260 Infinity II instrument from Agilent Technologies (Santa Clara, CA) and an LC–MS column (Agilent Technologies, Poroshell 120, SB C18-reversed-phase, length 50 mm, internal diameter: 2.1 mm, particle size: 2.7 micron) with a gradient of 10–95% v/v MeCN (0.1% v/v formic acid) in water (0.1% v/v formic acid) over 10 min. High-resolution mass spectrometry (HRMS) was performed with an AccuTOF 4G LC-plus from JEOL (Peabody, MA) equipped with an intense DART (Direct Analysis in Real Time) source.

No unexpected or unusually high safety hazards were encountered during the reported work.

1.3. Biological Reagents and Instrumentation

All procedures were performed at ambient temperature (~22 °C) and pressure (~1.0 atm) unless indicated otherwise. RNase A (product #R6513-50MG; ≥79 Kunitz units mg⁻¹) was from Sigma–Aldrich. RNase 1 concentrations were determined using a DS-11 UV–vis spectrophotometer from DeNovix (Wilmington, DE) and validated using a BCA assay (Smith et al. 1985) with a kit from Thermo Fisher Scientific (product #23227). Cell lysis was done using a benchtop cell disruptor from Constant Systems (Kennesaw, GA). Dialysis tubing was from Spectrum Labs (Rancho Dominguez, CA). Contaminating OVS was removed from MES buffer by anion-exchange chromatography (Smith et al. 2003). Fluorescence and absorbance measurements for enzyme kinetics were made with a Spark plate reader from Tecan (Männedorf, Switzerland). Clear 96-well half area, UV-star plates (product #675801) from Greiner (Monroe, NC) were used for absorbance

assays. Dinucleotide extinction coefficients were assessed with the DS-11 UV-vis spectrophotometer, which uses a variable path length and automatically scales the absorbance to a path length of 1 cm in the output. BL21(DE3) cells (product #69450-3) were from Sigma–Aldrich and were expanded to make electrocompetent cells. Crystals were seeded using a Seeding Tool (product #HR8-133) from Hampton Research (Aliso Viejo, CA).

2. Synthesis

2',5'-Di(t-butyldimethylsilyl)uridine (1a)

The synthetic procedure was adapted from Ogilvie and coworkers (Hakimelahi et al. 1982).

Uridine (3.00 g, 12.3 mmol) was dissolved in anhydrous THF (100 mL). Silver nitrate (4.59 g, 27.0 mmol) and TBSCl (4.07 g, 27.0 mmol) were added to the resulting solution. Then, pyridine (4.96 mL, 61.4 mmol) was added. The reaction mixture was stirred for 12 h in the dark. The reaction mixture was filtered over celite, washed with EtOAc (3×50 mL), and concentrated under reduced pressure. The crude product was purified by flash chromatography ($5:1\rightarrow1:1$ hexanes/EtOAc). Product **1a** was obtained as a colorless oil (4.83 g, 10.2 mmol, 83%).

All analytical data were in accordance with the literature (Razkin et al. 2007).

2',5'-Di(t-butyldimethylsilyl)-pseudouridine (1b)

Pseudouridine (2.00 g, 8.2 mmol) was dissolved in anhydrous THF (75 mL). Silver nitrate (3.06 g, 18.0 mmol) and TBSCl (2.72 g, 18.0 mmol) were added to the resulting solution. Then, pyridine (3.31 mL, 40.9 mmol) was added. The reaction mixture was stirred for 12 h in the dark. The reaction mixture was filtered over celite and washed with EtOAc (3×50 mL). The reaction mixture was concentrated under reduced pressure. The crude product was purified by flash chromatography ($5:1\rightarrow1:1$ hexanes/EtOAc). Product **1b** was obtained as a colorless oil (2.01 g, 4.3 mmol, 52%).

¹H NMR (CDCl₃, 500 MHz, δ): 9.33 (m, 1H), 9.10 (m, 1H), 7.70 (dd, 1H, J = 5.9, 1.2 Hz), 4.78 (dd, 1H, J = 2.4, 1.2 Hz), 4.18 (dd, 1H, J = 4.7, 2.4 Hz), 4.07 (ddd, 1H, J = 9.0, 7.3, 4.7 Hz), 3.99 (m, 1H), 3.86 (dt, 1H, J = 7.3, 2.6 Hz), 3.80 (dd, 1H, J = 11.5, 2.6 Hz), 2.42 (d, 1H, J = 9.0 Hz), 0.93 (s, 9H), 0.91 (s, 9H), 0.22 (s, 3H), 0.14 (s, 3H), 0.11 (s, 3H), 0.08 (s, 3H). ¹³C{¹H} NMR

(CDCl₃, 126 MHz, δ): 162.6, 152.1, 138.8, 113.5, 83.1, 79.3, 76.5, 70.1, 62.2, 26.1, 26.0, 18.6, 18.2, 0.1, -4.23, -5.2, -5.22, -5.30.

2',5'-Di(t-butyldimethylsilyl)- N^1 -methylpseudouridine (1c)

 N^1 -Methylpseudouridine (2.00 g, 7.8 mmol) was dissolved in anhydrous THF (75 mL). Silver nitrate (2.57 g, 17.0 mmol) and TBSCl (2.89 g, 17.0 mmol) were added to the resulting solution. Then, pyridine (3.93 mL, 38.7 mmol) was added. The reaction mixture was stirred for 12 h in the dark. The reaction mixture was filtered over celite and washed with EtOAc (3 × 50 mL). The reaction mixture was concentrated under reduced pressure. The crude product was purified by flash chromatography (5:1 \rightarrow 1:1 hexanes/EtOAc). Product **1c** was obtained as a colorless oil (1.36 g, 2.8 mmol, 36%).

¹H NMR (CDCl₃, 500 MHz, δ): 8.82 (s, 1H), 7.52 (d, 1H, J = 1.2 Hz), 4.79 (dd, 1H, J = 2.5, 1.2 Hz), 4.16 (dd, 1H, J = 4.8, 2.5 Hz), 4.07–3.99 (m, 2H), 3.87 (dt, 1H, J = 7.3, 2.4 Hz), 3.81 (dd, 1H, J = 11.6, 2.7 Hz), 3.35 (s, 3H), 2.44 (d, 1H, J = 8.9 Hz,), 0.93 (s, 9H), 0.92 (s, 9H), 0.23 (s, 3H), 0.14 (s, 3H), 0.12 (s, 3H), 0.11 (s, 3H). ¹³C{¹H} NMR (CDCl₃, 126 MHz, δ): 162.4, 150.9, 142.9, 113.2, 82.9, 79.1, 70.0, 62.1, 36.3, 26.1, 25.9, 18.7, 18.1, -4.3, -5.19, -5.22, -5.27.

2',3',5'-Tri(t-butyldimethylsilyl)adenosine (4)

Adenosine (3.00 g, 11.1 mmol) was suspended in DMF (20 mL). Imidazole (6.83 g, 100.3 mmol) and TBSCl (7.56 g, 50.1 mmol) were added, and the reaction mixture was stirred overnight. The reaction was stopped by the addition of H₂O (50 mL). The reaction mixture was extracted with EtOAc (3 × 100 mL). The combined organic phases were washed with 0.5 M hydrochloric acid (3 × 30 mL), saturated sodium bicarbonate solution (3 × 30 mL), and brine (40 mL). The organic phases were dried over Na₂SO₄(s) and concentrated under reduced pressure. The crude product was purified by flash chromatography (3:1 hexanes/EtOAc→EtOAc). Product 4 was obtained as a colorless solid (5.86 g, 9.57 mmol, 86%).

All analytical data were in accordance with the literature (Hisamatsu et al. 2006).

2',3'-Di(t-butyldimethylsilyl)adenosine (3)

Compound 4 (3.00 g, 4.9 mmol) was dissolved in aqueous acetic acid (50 mL, 80% v/v), and the resulting solution was stirred at 100 °C for 3 h. The reaction mixture was concentrated under reduced pressure to an oil and purified by flash chromatography (3:1 hexanes/EtOAc→EtOAc). Product 3 was obtained as a colorless solid (1.92 g, 3.87 mmol, 79%).

All analytical data were in accordance with the literature (Kotch et al. 2003).

Uridine Phosphoramidite (2a)

Compound **1a** (800 mg, 1.7 mmol) was dissolved in THF (5 mL). 2-Cyanoethyl N,N,N',N'-tetraisopropylphosphorodiamidite (537 μ L, 1.7 mmol) was added. Tetrazol (3.42 mL, 450 mM in MeCN, 1.5 mmol) was added and the reaction was stirred overnight at 40 °C. The reaction was stopped by the addition of a saturated aqueous solution of NaHCO₃ (5 mL). The mixture was extracted with EtOAc (3 × 10 mL). The combined organic phases were dried over Na₂SO₄(s) and concentrated under reduced pressure. The crude product was purified by flash chromatography (3:1 hexanes/EtOAc \rightarrow EtOAc). Product **2a** was obtained as a colorless oil that was a mixture of diastereomers (883 mg, 1.31 mmol, 85%).

³¹P{¹H} NMR (CDCl₃, 202 MHz, δ): 150.9, 149.9. HRMS–ESI (m/z): [M + H⁺] calcd for C₂₄H₄₅N₃O₈PSi₂, 590.2477; found, 590.2485 (hydrolyzed).

Pseudouridine Phosphoramidite (1b)

Compound **1b** (330 mg, 698 μ mol) was dissolved in THF (4 mL). 2-Cyanoethyl N,N,N',N'-tetraisopropylphosphorodiamidite (221 μ L, 698 μ mol) was added. Then, tetrazol (1.4 mL, 450 mM

in MeCN, 634 μ mol) was added and the reaction was stirred overnight at 40 °C. The reaction was stopped by the addition of a saturated aqueous solution of NaHCO₃ (5 mL). The mixture was extracted with EtOAc (3 × 10 mL). The combined organic phases were dried over Na₂SO₄(s) and concentrated under reduced pressure. The crude product was purified by flash chromatography (EtOAc \rightarrow 3:1 hexanes/EtOAc). Product **2b** was obtained as a colorless oil that was a mixture of diastereomers (273 mg, 406 μ mol, 64%). Due to its limited stability, the product was characterized only by ³¹P NMR and used immediately in the next synthetic step.

³¹P{¹H} NMR (CDCl₃, 202 MHz, δ): 149.9, 148.6. HRMS–ESI (m/z): [M + H⁺] calcd for C₂₄H₄₅N₃O₈PSi₂, 590.2477; found, 590.2466 (hydrolyzed).

N¹-Methylpseudouridine Phosphoramidite (2c)

Compound 1c (650 mg, 1.3 mmol) was dissolved in THF (7 mL). 2-Cyanoethyl *N*,*N*,*N*',*N*'-tetraisopropylphosphorodiamidite (428 μL, 1.34 mmol) was added to the resulting solution. Then, tetrazol (2.7 mL, 450 mM in MeCN, 1.2 mmol) was added. The reaction mixture was stirred overnight at 40 °C. The reaction was stopped by the addition of a saturated aqueous solution of NaHCO₃ (8 mL). The mixture was extracted with EtOAc (3 × 15 mL). The combined organic phases were dried over Na₂SO₄(s) and concentrated under reduced pressure. The crude product was purified by flash chromatography (3:1 hexanes/EtOAc→EtOAc). Product 2c was obtained as a colorless oil that was a mixture of diastereomers (558 mg, 812 μmol, 67%). Do to its limited stability, the product was characterized only by ³¹P NMR spectroscopy and used immediately in the next synthetic step.

 $^{31}P\{^{1}H\}$ NMR (CDCl₃, 202 MHz, δ): 149.7, 148.9. HRMS–ESI (m/z): [M + H⁺] calcd for $C_{31}H_{60}N_{4}O_{7}PSi_{2}$, 687.3733; found, 687.3741.

Protected Uridylyl(3'→5')adenosine (5a)

Phosphoramidite 2a (100 mg, 148 μmol) and compound 3 (88 mg, 178 μmol) were dissolved in THF (2 mL). Tetrazole (495 μL, 450 mM in MeCN, 223 μmol) was added to the resulting solution, and the reaction mixture was stirred at 40 °C overnight. The reaction mixture was cooled to room temperature. I₂ (38 mg, 148 μmol) was dissolved in 2:1 THF/H₂O (2 mL), and the resulting solution was added to the reaction mixture. The reaction mixture was stirred for 15 min at room temperature. The reaction was stopped by the addition of an aqueous solution of sodium bisulfite (1 mL, 10% w/v). The reaction mixture was extracted with DCM (3 × 4 mL) The combined organic phases were dried over Na₂SO₄(s) and concentrated under reduced pressure. The crude product was purified by flash chromatography (DCM→9:1 DCM/methanol). Product 5a was obtained as a colorless oil that was a mixture of diastereomers (76 mg, 70 μmol, 47%).

¹H NMR (CDCl₃, 500 MHz, δ): 10.24 (s), 8.86 (s), 8.44 (s), 8.41 (s), 8.07 (d, J = 1.5 Hz), 7.79 (d, J = 8.1 Hz), 7.68 (d, J = 8.2 Hz), 7.52 (m), 6.95 (s), 6.90 (s), 6.12 (d, J = 7 Hz), 5.96 (d, J = 7.0 Hz), 5.89 (m,), 5.84 (m), 5.69 (m), 5.00 (m), 4.81 (m), 4.75 (m), 4.70–4.66 (m), 4.51–4.08 (m), 4.07–3.96 (m), 3.88 (m), 3.81 (m), 3.66–3.49 (m), 2.80–2.63 (m), 0.99–0.75 (m), 0.17–0.04 (m). ¹³C{¹H} NMR (CDCl₃, 126 MHz, δ): 164.1, 162.9, 156.1, 153.0, 151.3, 151.0, 149.3, 142.9, 119.8, 116.3, 113.3, 102.92, 90.4, 86.3, 83.0, 82.1, 79.0, 74.3, 70.1, 62.9, 62.2, 36.2, 26.0, 26.0, 25.9, 25.8, 25.5, 18.6, 18.3, 18.1, 18.0, 17.9, 17.9, -4.2, -4.3, -4.5, -4.6, -4.9, -5.1, -5.2, -5.4, -5.6. ³¹P{¹H} NMR (CDCl₃, 202 MHz, δ): -1.64, -1.81. HRMS–ESI (m/z): [M + H⁺] calcd for C₄₆H₈₄N₈O₁₂PSi₄, 1083.5018; found, 1083.5012.

Protected Pseudouridylyl(3'→5')adenosine (5b)

Phosphoramidite **2b** (250 mg, 372 μmol) and **4** (221 mg, 445 μmol) were dissolved in THF (2 mL). Tetrazole (1.2 mL, 450 mM in MeCN, 540 μmol) was added to the resulting solution, and the reaction mixture was stirred at 40 °C overnight. The reaction mixture was cooled to room temperature. I₂ (94 mg, 371 μmol) was dissolved in 2:1 THF/H₂O (4 mL), and the resulting solution was added to the reaction mixture. The reaction mixture was stirred for 15 min at room temperature. The reaction was stopped by the addition of an aqueous solution of sodium bisulfite (2 mL, 10% w/v). The reaction mixture was extracted with DCM (3 × 8 mL). The combined organic phases were dried over Na₂SO₄(s) and concentrated under reduced pressure. The crude product was purified by flash chromatography (DCM→9:1 DCM:methanol). Product **5b** was obtained as a colorless oil that was a mixture of diastereomers (209 mg, 193 μmol, 52%).

¹H NMR (CDCl₃, 500 MHz, δ): 9.23 (s), 8.63 (s), 8.39–8.29 (m), 8.21–7.77 (m), 7.59–7.31 (m), 5.87 (m), 5.73 (s), 5.21 (d), 5.02 (s, 2H), 4.87–4.16 (m), 3.58 (m), 3.22 (d, J = 11.2 Hz, 1H), 3.11–2.90 (m), 2.85–2.61 (m), 0.98–0.63 (m), 0.24–0.15 (m). ¹³C{¹H} NMR (CDCl₃, 126 MHz, δ): 163.5, 156.0, 152.6, 152.3, 151.6, 149.5, 149.4, 143.9, 142.9, 141.5, 140.7, 139.9, 120.6, 120.2, 116.7, 116.3, 113.5, 112.5, 90.8, 89.8, 82.9, 82.3, 79.4, 74.1, 72.2, 71.3, 67.1, 62.8, 62.5, 62.2, 53.5, 36.0, 26.1, 25.9, 25.9, 25.8, 25.8, 25.7, 25.7, 19.6, 19.6, 18.50, 18.2, 18.2, 18.1, 18.1, 17.9, -4.2, -4.3, -4.5, -4.6, -4.6, -4.6, -4.7, -4.8, -4.8, -4.9, -5.1, -5.2, -5.3, -5.5. ³¹P{¹H} NMR (CDCl₃, 202 MHz, δ): -2.40. HRMS–ESI (m/z): [M + H⁺] calcd for C₄₆H₈₄N₈O₁₂PSi₄, 1083.5018; found, 1083.5004.

Protected N^1 -Methylpseudouridylyl(3' \rightarrow 5')adenosine (5c)

Phosphoramidite **2c** (200 mg, 291 μmol) and **4** (173 mg, 349 μmol) were dissolved in THF (2 mL). Tetrazole (970 μL, 450 mM in MeCN, 437 μmol) was added to the resulting solution, and the reaction mixture was stirred overnight at 40 °C. The reaction was cooled to room temperature. I₂ (74 mg, 291 μmol) was dissolved in 2:1 THF/H₂O (4 mL), and the resulting solution was added to the reaction mixture. The reaction mixture was stirred for 15 min at room temperature. The reaction was stopped by the addition of an aqueous solution of sodium bisulfite (2 mL, 10% w/v). The reaction mixture was extracted with DCM (3 × 8 mL) The combined organic phases were dried over Na₂SO₄(s) and concentrated under reduced pressure. The crude product was purified by flash chromatography (DCM→9:1 DCM/methanol). Product **5c** was obtained as a colorless oil that was a mixture of diastereomers (181 mg, 165 μmol, 57%).

¹H NMR (CDCl₃, 500 MHz, δ): 9.24 (s), 8.37 (s), 8.01 (s), 7.96 (s), 7.37 (s), 7.26 (s), 7.23 (s), 6.91 (s), 5.89 (d, J = 4.6 Hz), 5.77 (d, J = 3.7 Hz), 4.97 (m), 4.83 (d), 4.75 (s, 2H), 4.69 (m), 4.62 (d, J = 5.5 Hz), 4.57 (d, J = 7.8 Hz), 4.49–4.19 (m), 3.85 (m), 3.78 (s), 3.69 (s), 3.43 (m), 3.38 (s), 2.89 (m), 2.70 (m), 0.95–0.89 (m), 0.87–0.78 (mm), 0.08 (m), -0.01 (m). ¹³C{¹H} NMR (CDCl₃, 126 MHz, δ): 163.1, 156.3, 155.8, 152.9, 149.0, 144.2, 135.3, 116.6, 91.9, 83.3, 79.7, 74.2, 73.6, 72.2, 70.5, 62.4, 62.0, 60.4, 53.4, 47.9, 26.0, 25.8, 25.8, 25.7, 19.5, 19.4, 19.1, 18.2, 18.0, 17.9, 17.9, 1.0, -4.4, -4.7, -5.0, -5.1, -5.6. ³¹P{¹H} NMR (CDCl₃, 202 MHz, δ): -1.94, -2.12. HRMS–ESI (m/z): [M + H⁺] calcd for C₄₇H₈₆N₈O₁₂PSi₄, 1097.5174; found, 1097.5182.

Uridylyl(3'→5')adenosine·NEt₃

Compound **5a** (20 mg, 18 μ mol) was dissolved in in 2:1 ammonium hydroxide/ethanol (2 mL), and the resulting solution was stirred at 55 °C overnight. The reaction mixture was concentrated under reduced pressure. The resulting oil was taken up in THF (1 mL), TBAF (369 μ L, 369 μ mol, 1 M in THF) was added, and the resulting mixture was stirred for 48 h at room temperature. The reaction mixture was diluted twofold with H₂O, the THF was removed under reduced pressure, and the aqueous solution was extracted with diethyl ether (1 × 3 mL). Any ether dissolved in the aqueous layer was removed under reduced pressure. A HiTrap Q HP anion-exchange column was charged with the nucleotide, which was eluted with a linear gradient of 0–40% v/v triethylammonium bicarbonate buffer, pH 8. UpA eluted soon after the beginning of the gradient. The fractions containing UpA were concentrated under reduced pressure to an oil. The oil was dissolved in a minimal amount of MeOH, and EtOAc was added to precipitate the dinucleotide. The solution was stored at -20 °C overnight to complete precipitation. The precipitate was dried, and lyophilization yielded the triethylammonium salt of UpA as a fluffy white solid (4.5 mg, 7.9 μ mol, 43%).

¹H NMR (D₂O, 400 MHz, δ): 8.44 (s, 1H), 8.26 (s, 1H), 7.76 (d, 1H, J = 8.1 Hz,), 6.12 (d, 1H, J = 4.7 Hz), 5.78 (d, 1H, J = 8.1 Hz), 5.73 (d, 1H, J = 4.5 Hz), 4.72 (pt, 1H, J = 4.9 Hz,), 4.54 (pt, 1H, J = 5.1 Hz,), 4.47 (m, 1H), 4.37 (m, 1H), 4.31–4.21 (m, 2H), 4.17 (m, 3H), 3.79 (dd, 1H, J = 12.9, 2.8 Hz), 3.73 (dd, 1H, J = 12.9, 3.9 Hz), 3.21 (q, 6H, J = 7.3 Hz), 1.37–1.13 (t, 9H, J = 7.3 Hz). ¹³C { ¹H } NMR (D₂O, 101 MHz, δ): 152.6, 146.5, 141.3, 139.6, 102.1, 89.2, 87.4, 74.0, 72.9, 69.8, 60.2, 46.7, 8.2. ³¹P NMR (D₂O, 162 MHz, δ): -0.73. HRMS–ESI (m/z): [M – H⁺] calcd for C₁₉H₂₃N₇O₁₂P, 572.1148; found, 572.1140.

Pseudouridylyl(3'→5')adenosine·NEt₃

Compound **5b** (30 mg, 28 μ mol) was dissolved in 2:1 ammonium hydroxide/ethanol (2 mL), and the resulting solution was stirred at 55 °C overnight. The reaction mixture was concentrated under reduced pressure. The resulting oil was taken up in THF (1 mL), and TBAF (414 μ L, 414 μ mol, 1 M in THF) was added, and the resulting mixture was stirred for 48 h at room temperature. The reaction mixture was diluted twofold with H₂O, the THF was removed under reduced pressure, and the aqueous solution was extracted with diethyl ether (1 × 3 mL). Any ether dissolved in the aqueous layer was removed under reduced pressure. A HiTrap Q HP anion-exchange column was charged with the nucleotide, which was eluted with a linear gradient of 0–40% v/v triethylammonium bicarbonate buffer, pH 8. Ψ pA eluted soon after the beginning of the gradient. The fractions containing Ψ pA were concentrated under reduced pressure to an oil. The oil was dissolved in a minimal amount of MeOH, and EtOAc was added to precipitate the dinucleotide. The solution was stored at -20 °C overnight to complete precipitation. The precipitate was dried, and lyophilization yielded the triethylammonium salt of Ψ pA as a fluffy white solid (7.45 mg, 13.0 μ mol, 47%).

¹H NMR (D₂O, 500 MHz, δ): 8.48 (s, 1H), 8.32 (s, 1H), 7.55 (s, 1H), 6.13 (d, 1H, J = 4.3 Hz,), 4.64 (pt, 1H, J = 4.7 Hz,), 4.59 (d, 1H, J = 4.7 Hz), 4.51 (pt, 1H, J = 5.1 Hz), 4.40–4.36 (m, 1H), 4.36–4.32 (m, 1H), 4.26 (m, 1H), 4.22 (m, 1H), 4.13 (m, 1H), 4.09 (s, 1H), 3.79 (dd, 1H, J = 12.8, 2.8 Hz), 3.68 (dd, 1H, J = 12.8, 4.6 Hz), 3.18 (q, 6H, J = 7.3 Hz), 1.25 (td, 9H, J = 7.3) ¹³C { ¹H } NMR (D₂O, 126 MHz, δ): 149.6, 148.5, 140.9, 140.5, 110.2, 87.9, 83.3, 81.8, 79.4, 74.4, 72.5, 69.6, 64.3, 60.9, 46.7, 8.2. ³¹P { ¹H } NMR (D₂O, 202 MHz, δ): 0.08. HRMS–ESI (m/z): [M – H⁺] calcd for C₁₉H₂₃N₇O₁₂P, 572.1148; found, 572.1157.

N^1 -Methylpseudouridylyl(3' \rightarrow 5')adenosine (m¹ Ψ pA)

Compound **5c** (50 mg, 46 μ mol) was dissolved in 2:1 ammonium hydroxide/ethanol (3 mL), and the resulting solution was stirred at 55 °C overnight. The reaction mixture was concentrated under reduced pressure. The resulting oil was taken up in THF (1.5 mL), and TBAF (682 μ L, 682 μ mol, 1 M in THF) was added. The resulting mixture was stirred for 48 h at room temperature. The reaction mixture was diluted twofold with H₂O, the THF was removed under reduced pressure, and the aqueous solution was extracted with diethyl ether (1 × 3 mL). Any ether dissolved in the aqueous layer was removed under reduced pressure. A HiTrap Q HP anion-exchange column was charged with the nucleotide and eluted with a linear gradient from 0–40% v/v triethylammonium bicarbonate buffer, pH 8. m¹ΨpA eluted soon after the beginning of the gradient. The fractions containing m¹ΨpA were concentrated under reduced pressure to an oil. The oil was dissolved in a minimal amount of MeOH, and EtOAc was added to precipitate the dinucleotide. The solution was stored at -20 °C overnight to complete the precipitation. The precipitate was dried and lyophilization yielded the triethylammonium salt of **m**¹ΨpA as a fluffy white solid (11 mg, 19 μ mol, 41%).

¹H NMR (D₂O, 500 MHz, δ): 8.47 (s, 1H,), 8.30 (s, 1H), 7.66 (s, 1H), 6.13 (d, 1H, J = 4.3 Hz), 4.64 (pt, 1H, J = 4.7 Hz), 4.61 (d, 1H, J = 4.6 Hz), 4.52 (pt, 1H, J = 5.2 Hz), 4.42 (m, 1H), 4.36 (m, 1H), 4.31–4.27 (m, 1H), 4.25 (t, 1H, J = 4.9 Hz), 4.15 (dt, 1H, J = 11.8, 3.6 Hz), 4.13–4.08 (m, 1H), 3.82 (dd, 1H, J = 12.8, 2.8 Hz), 3.71 (dd, 1H, J = 12.8, 4.5 Hz), 3.33 (s, 3H), 3.20 (q, 6H, J = 7.3 Hz), 1.28 (t, 9H, J = 7.3 Hz). ¹³C{¹H} NMR (D₂O, 126 MHz, δ): 164.3, 153.8, 152.0, 150.4, 148.5, 145.6, 140.1, 118.6, 110.3, 87.9, 83.0, 81.8, 79.3, 74.4, 74.0, 72.6, 69.4, 64.2, 60.8, 46.6, 45.1, 36.0, 8.2. ³¹P{¹H} NMR (D₂O, 202 MHz, δ): -0.48. HRMS–ESI (m/z): [M – H⁺] calcd for C₂₀H₂₅N₇O₁₂P, 586.1304; found, 586.1315.

3. Heterologous Production and Purification of RNase 1

3.1. SDS-PAGE and LC-MS of RNase 1

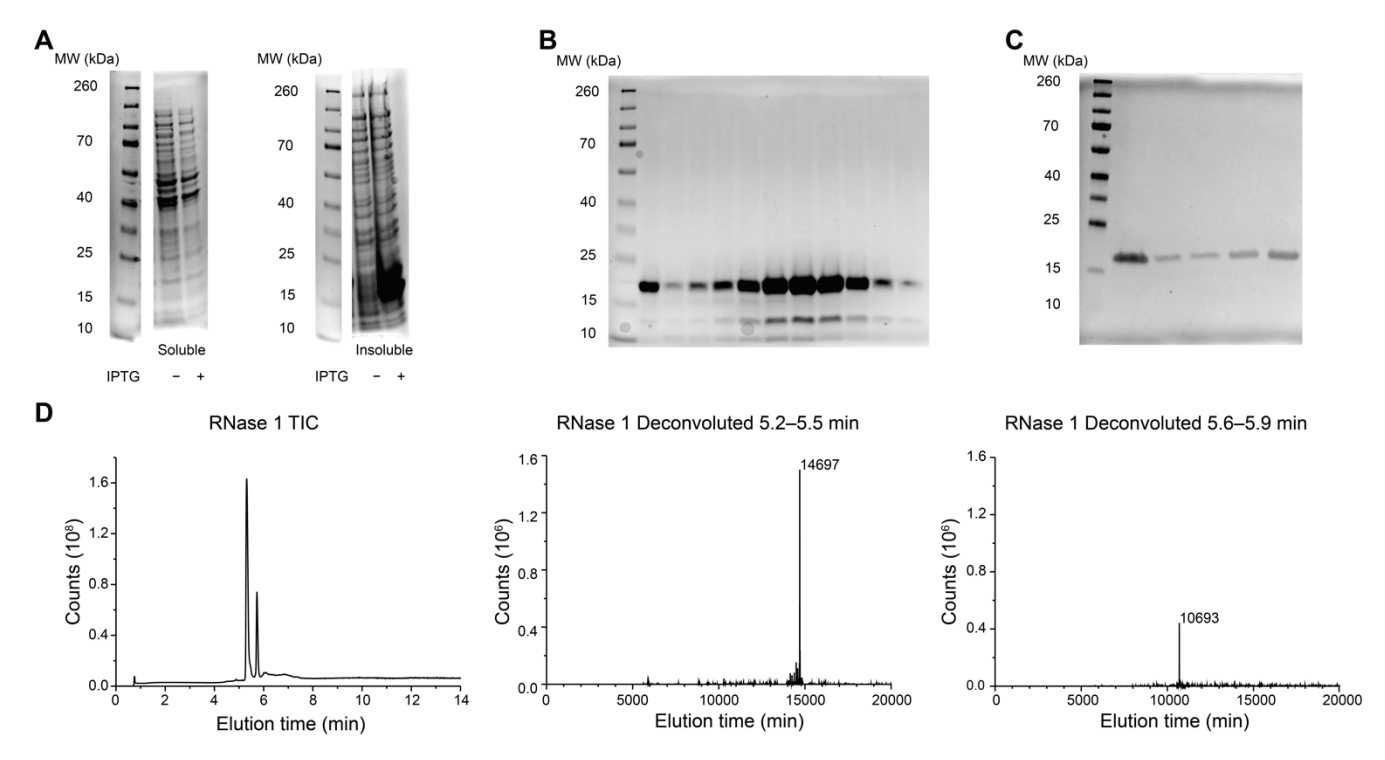


FIGURE S1. (A) SDS-PAGE gel for the heterologous production of human RNase 1. Human RNase 1 is present in the insoluble fraction after 3 h of induction with IPTG. (B) SDS-PAGE gel of protein-containing fractions from cation-exchange chromatography. (C) Gel of subsequent buffer exchange and concentration, which led to the loss of lower molecular weight species. (D) QTOF-MS of RNase 1 used for assays of enzymatic activity. RNase 1 was present at the expected molecular weight (14,697 Da) with a minor contaminant at 10,093 Da that was not apparent from SDS-PAGE analysis.

3.2. Activity Validation of Commercial RNase A and Recombinant RNase 1

An assay with a hypersensitive FRET substrate, FAM–dArUdAdA–6-TAMRA (Fig. S2), was used to ensure that the purified RNase 1 and commercial RNase A were active catalysts of RNA cleavage (Kelemen et al. 1999; Wralstad and Raines 2024). Assays were carried out in the same buffers as those of dinucleotide cleavage (RNase A: 0.10 M OVS-free MES–NaOH, pH 6.0, containing 0.10 M NaCl; RNase 1: 0.10 M Tris–HCl, pH 7.5, 0.10 M NaCl) with 12.5 pM of enzyme and 200 nM of FAM–dArUdAdA–6-TAMRA. Fluorescence intensity (*I*) was measured with a Tecan Spark microplate reader, monitoring emission at $\lambda_{em} = 515$ nm after excitation at $\lambda_{ex} = 493$ nm with a 5-nm bandwidth. Assays were performed with 5 replicates in a flat, black, halfarea 96-well plate. Assuming a linear relationship for substrate conversion to product and in the initial rates region of Michaelis–Menten kinetics and that assays are performed at a substrate concentration well below the $K_{\rm M}$, which we estimated to be 22 μ M for RNase A (Kelemen et al. 1999), the following relationship was used to determine catalytic efficiency via linear regression:

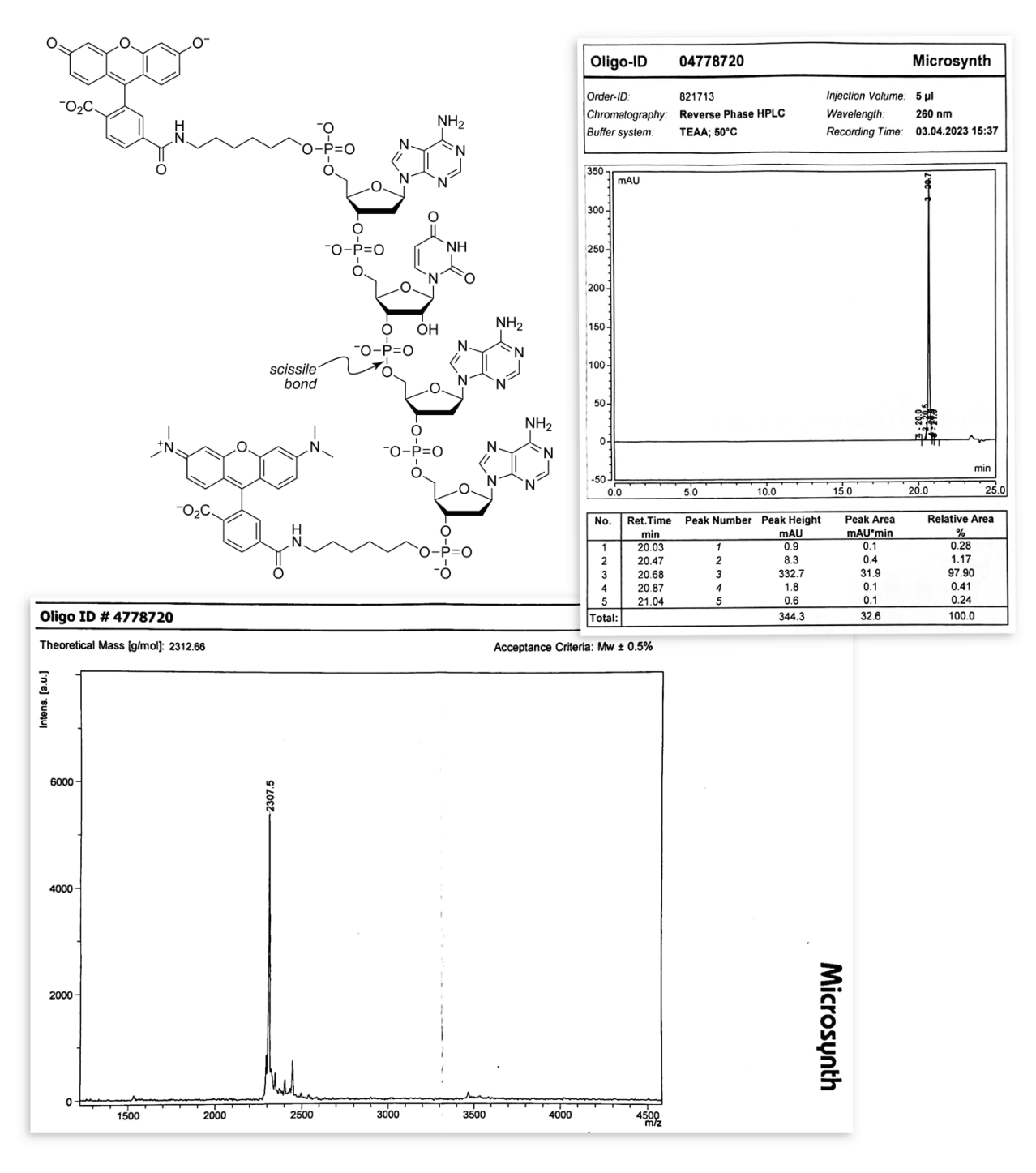


FIGURE S2. Structure of 6-FAM–dArU(dA)₂–6-TAMRA, which is a hypersensitive fluorogenic substrate for assays of ribonucleolytic activity (Kelemen et al. 1999; Wralstad and Raines 2024). The cleavage of the scissile bond increases the fluorescence of the FAM moiety with $\lambda_{ex} = 493 \pm 5$ nm and $\lambda_{em} = 515 \pm 5$ nm. Insets: reversed-phase HPLC chromatogram (top) and MALDI–TOF mass spectrum (bottom) of synthetic 6-FAM–dArU(dA)₂–6-TAMRA.

$$\frac{(I-I_0)}{(I_{\text{max}}-I_0)} = \frac{[\text{product}]_t}{[\text{substrate}]_0} = \frac{k_{\text{cat}}}{K_{\text{M}}} [\text{enzyme}] t \tag{1}$$

 I_0 was determined by measuring the fluorescence intensity before the addition of a ribonuclease, and $I_{\rm max}$ was determined by measuring the fluorescence intensity after the addition of excess RNase A (5 μ M). The resulting values of $k_{\rm cat}/K_{\rm M}$ are listed in Table S1 along with literature values using a similar substrate.

TABLE S1. Values of k_{cat}/K_{M} for the cleavage of FAM–dArUdAdA–6-TAMRA (Fig. S2) by RNase A and RNase 1

Ribonuclease	рН	$k_{\rm cat}/K_{\rm M}~(10^6~{ m M}^{-1}~{ m s}^{-1})$	Literature $k_{\text{cat}}/K_{\text{M}}$ (10 ⁷ M ⁻¹ s ⁻¹)
RNase A	6.0	19.5 ± 2.7	25 ± 3 (Kelemen et al. 1999)
	7.5	2.28 ± 0.18	_
RNase 1	6.0	0.65 ± 0.05	_
	7.5	5.11 ± 0.51	9.5 ± 0.3 (Sayers et al. 2021)

4. Experimentally Derived Extinction Coefficients of UpA, ΨpA, and m¹ΨpA

Extinction coefficients were derived to determine the concentration of solutions of synthetic UpA, Ψ pA, and m¹ Ψ pA. In short, >10 mg of each dinucleotide was weighed out on an analytical balance and dissolved in water to a concentration of 2 mg/mL. This solution was then diluted 1:20 into water, and the absorbance was measured at 260 nm using 1 μ L volumes (n = 5 technical replicates). Extinction coefficients were calculated using the Beer–Lambert law: $A_{260 \text{ nm}} = \varepsilon_{260 \text{ nm}} \cdot l \cdot c$. where $A_{260 \text{ nm}}$ is the absorbance at 260 nm, $\varepsilon_{260 \text{ nm}}$ is the extinction coefficient at 260 nm, l is the path length, and c is the concentration of dinucleotide. The resulting values of $\varepsilon_{260 \text{ nm}}$ were UpA, 19770 \pm 750 cm⁻¹ M⁻¹; Ψ pA, 17890 \pm 440; and m¹ Ψ pA, 17910 \pm 200. The higher value for UpA is consistent with the known hypochromicity of Ψ and m¹ Ψ (Finol et al. 2024). The value of $\varepsilon_{260 \text{ nm}}$ for UpA was 25% less than that in an early report (Beaven et al. 1955).

We also evaluated how the overall spectra in the UV range differed for each substrate. These were obtained using 800 μ M of substrate in 100 mM MES–NaOH buffer, pH 6.0, containing NaCl (100 mM) or 100 mM Tris–HCl buffer, pH 7.5, containing NaCl (100 mM) with absorbance scanned over 220 nm to 320 nm. In general, the spectrum of each substrate is similar, though that of m¹ Ψ pA is shifted slightly toward longer wavelengths, as shown in Fig. S3. There were no noticeable differences due to buffer or pH differences.

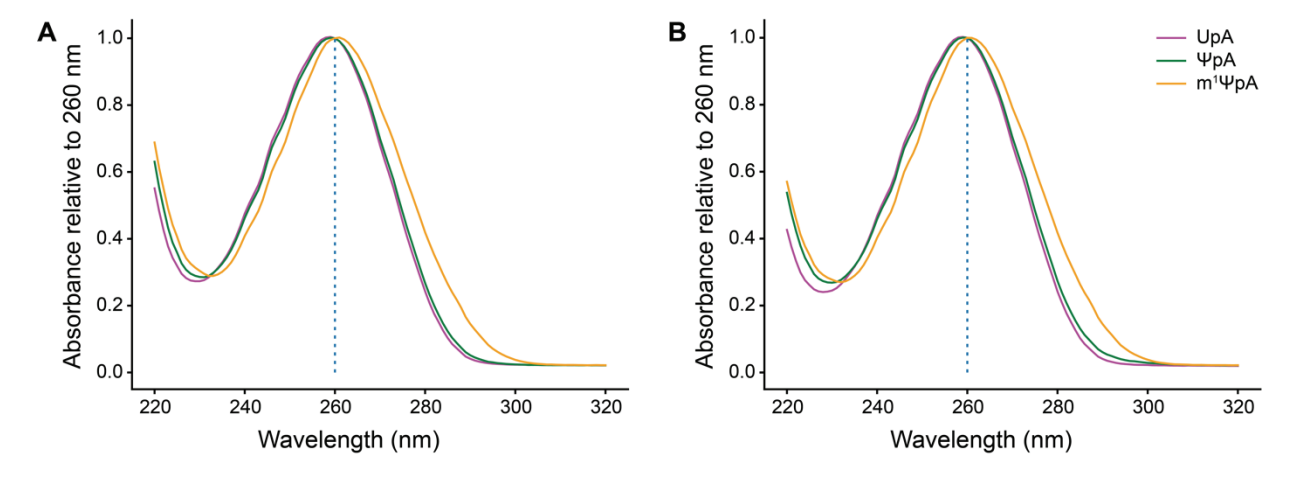


FIGURE S3. UV spectra of UpA, Ψ pA, and m¹ Ψ pA at pH 6.0 (*A*) and pH 7.5 (*B*). Spectra are shown as the mean (n = 4 technical replicates) normalized to the absorbance at 260 nm.

5. UV Spectra of UpA, ΨpA, and m1 ΨpA

Previous reports on what wavelength to use for UpA cleavage assays vary. For each substrate and buffer condition, we obtained UV spectra and examined changes in absorbance after cleavage to select a wavelength that had the highest sensitivity. These examinations were done prior to kinetic assays, where a scan of absorbances between 220 and 320 nm with 1 nm increments was performed before and after the addition of enzyme. The spectra of the scan of the initial substrate (no enzyme added) and the scan of the enzyme-saturated condition (with 2 μ M RNase A) were then averaged for each concentration of substrate, and the difference was subtracted to obtain the change in absorbance upon enzyme-catalyzed cleavage.

We sought a wavelength that had a large change in absorbance and was distal from the absorbance maximum, such that the absorbance change was directly proportional to substrate concentration, particularly at higher concentrations (Fig. S4). For assays in different buffers, we used the wavelength chosen for the enzyme–substrate pair at the optimal pH for catalysis. The wavelengths thus chosen for the enzyme-substrate pairs are listed in Table S2.

TABLE S2. Wavelength for kinetic assays of each enzyme–substrate pair

Substrate	RNase A	RNase 1
UpA	278 nm	276 nm
ΨрА	276 nm	276 nm
$m^1\Psi pA$	287 nm	287 nm

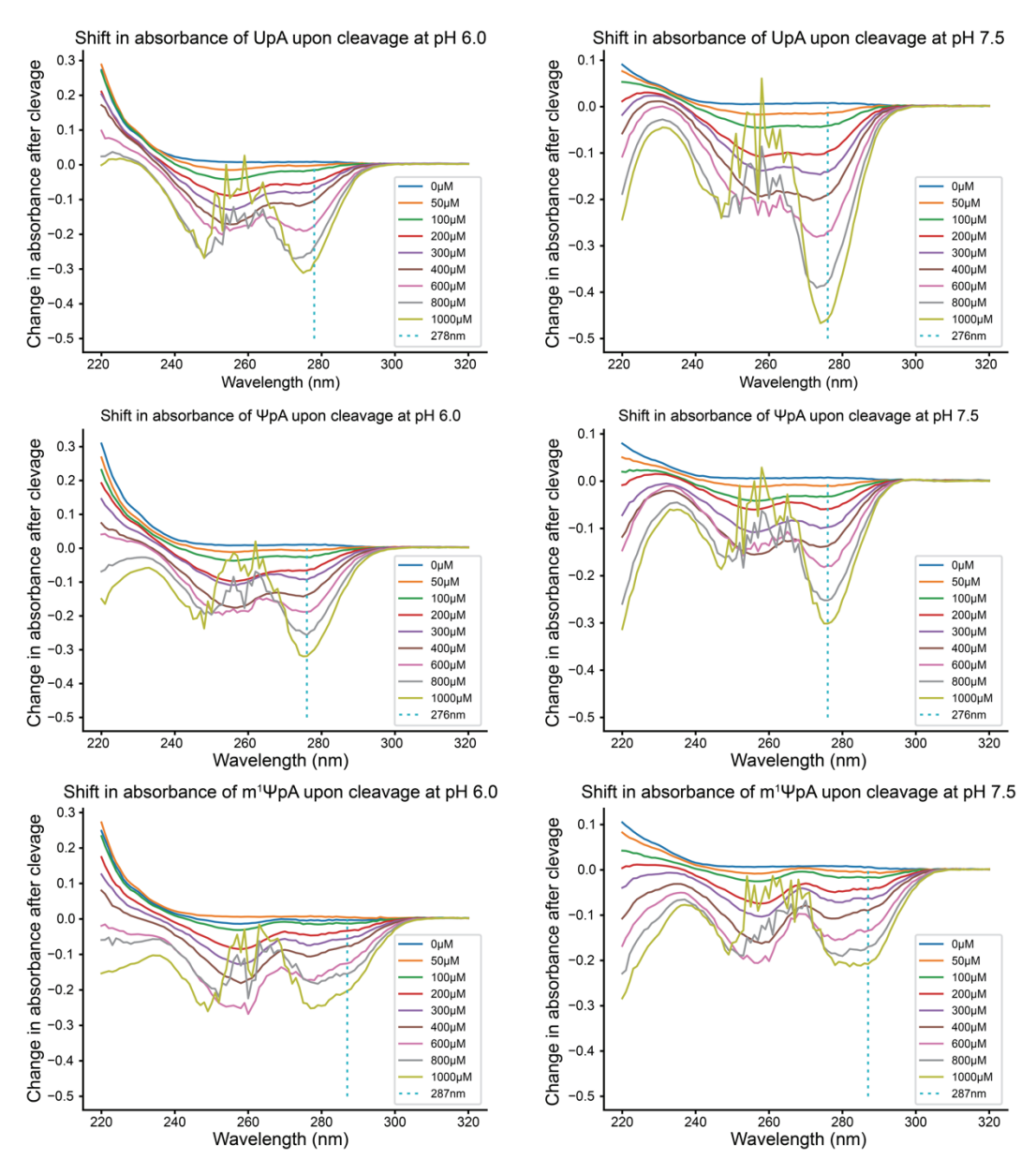


FIGURE S4. Shift in absorbance due to the cleavage of UpA, Ψ pA, and m¹ Ψ pA at pH 6.0 and 7.5. The wavelengths used in kinetic measurements are indicated with a dotted line. Spectra are shown as the mean (n = 4 technical replicates).

6. Additional Kinetic Data for Catalysis of UpA, ΨpA, and m¹ΨpA Cleavage

To assess differences in catalysis, we generated plots of the rate normalized to enzyme concentration for each substrate (Fig. S5). RNase A is a better catalyst for the cleavage of each dinucleotide substrates, and RNase A and RNase 1 differed most in catalysis of UpA cleavage.

The raw data, the code used to fit these data, and the raw data for Fig. 2 can be accessed at https://github.com/clair-gutierrez/pseudouridine-rnase.

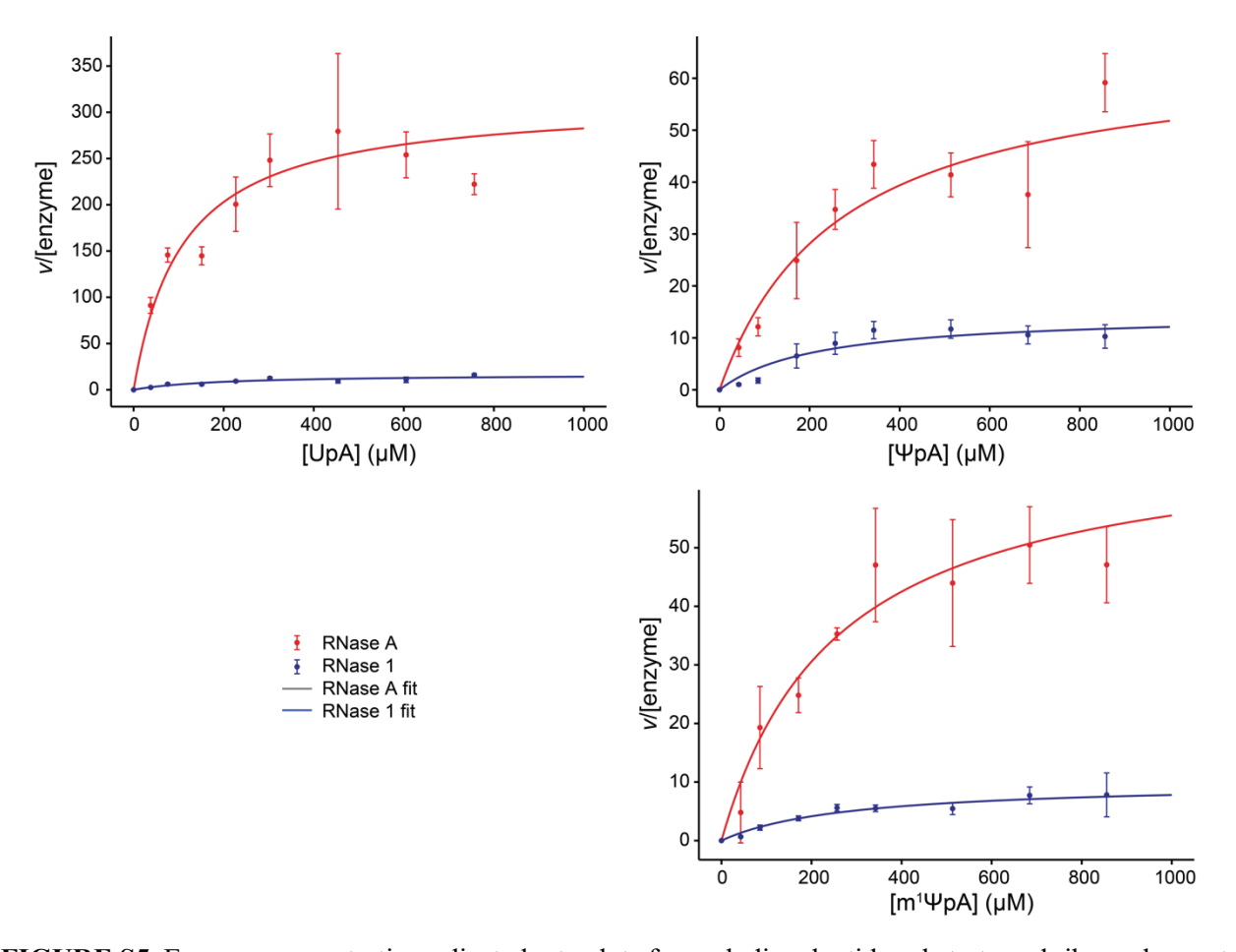


FIGURE S5. Enzyme concentration-adjusted rate plots for each dinucleotide substrate and ribonuclease at its optimal pH. Each data point is the mean \pm SD (n = 4 technical replicates).

7. Kinetic Data for Catalysis of UpA Cleavage at Different pHs

To understand how pH might affect the cleavage of the different substrates, we conducted kinetic assays for RNase A at pH 7.5 and RNase 1 at pH 6.0, which differ from the optimal pH values for catalysis. These assays were done using the same buffers and conditions as described in the Materials and Methods section for these pH values, switching only the enzymes. These suboptimal pH conditions resulted in large $K_{\rm M}$ values, making it difficult to obtain $k_{\rm cat}$ and $K_{\rm M}$ independently with accessible substrate concentrations (<1 mM). Instead, values of $k_{\rm cat}/K_{\rm M}$ were obtained in the [S] $\ll K_{\rm M}$ regime, where the Michaelis–Menten equation collapses to a linear equation:

$$\frac{\mathrm{d[P]}}{\mathrm{d}t} \approx \frac{k_{\mathrm{cat}}}{K_{\mathrm{M}}} [\mathrm{E}][\mathrm{S}]_{0} \tag{2}$$

In this regime, the accuracy in the values of $k_{\rm cat}$ and $K_{\rm M}$ is low, but the accuracy in their ratio is high (Bisswanger 2014). The data were fitted in two ways. First, the typical fit was done with the Michaelis–Menten equation, which provides $k_{\rm cat}$ and $K_{\rm M}$ independently, albeit with large errors, and those values were used to determine the ratio $k_{\rm cat}/K_{\rm M}$. Second, a linear fit was done by applying Eq 2 to kinetic data with $[S]_0 \le 300~\mu{\rm M}$. These latter values were used in Fig. 6.

TABLE S3. Values of $k_{\text{cat}}/K_{\text{M}}$ for the cleavage of UpA, Ψ pA, and m¹ Ψ pA by RNase A and RNase 1 at the optimal pH of the other enzyme. Values from the fit to the Michaelis–Menten equation and from the linear fit in the region of [S] $\ll K_{\text{M}}$ and are reported as the mean \pm SD for 4 technical replicates for each substrate condition.

Ribonuclease	рН	Substrate	$k_{\text{cat}}/K_{\text{M}} (10^5 \text{ M}^{-1} \text{ s}^{-1})$ Michaelis–Menten fit	$k_{\text{cat}}/K_{\text{M}} (10^5 \text{ M}^{-1} \text{ s}^{-1})$ linear fit
RNase A	7.5	UpA	1.36 ± 0.45	1.21 ± 0.07
	7.5	ΨрА	0.67 ± 0.78	0.69 ± 0.07
	7.5	$m^{l}\Psi pA$	0.36 ± 0.25	0.25 ± 0.02
RNase 1	6.0	UpA	0.68 ± 0.47	0.54 ± 0.02
	6.0	ΨрА	0.33 ± 0.24	0.33 ± 0.02
	6.0	$m^l\Psi pA$	0.36 ± 0.91	0.35 ± 0.01

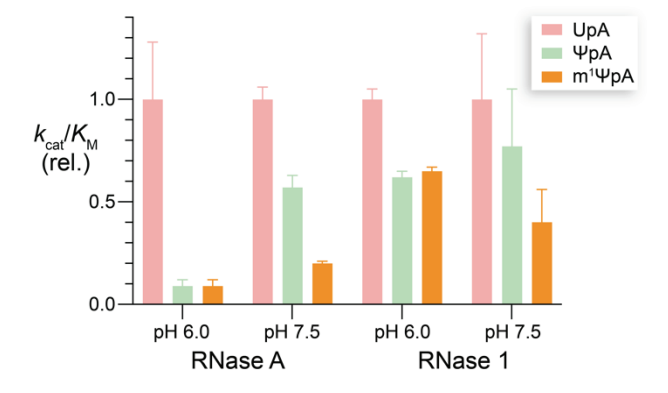


FIGURE S6. pH-Dependence of the relative $k_{\text{cat}}/K_{\text{M}}$ values for catalysis of the cleavage of dinucleotide substrates by RNase A and RNase 1 at 25 °C. Values are the mean \pm SD of 4 replicates.

8. Statistics for X-ray Crystallography

TABLE S4. Data collection, processing, and refinement statistics of the complexes of RNase A with U>v, Ψ >v, and $m^1\Psi$ >v*

	RNase A·U>v	RNase A·Ψ>v	RNase A·m¹Ψ>v
PDB code	9ncs	9o4v	9o5b
Wavelength (Å)	1.54	1.54	1.54
Resolution range (Å)	36.16–1.83	29.17–1.70	25.08-1.71
	(1.85-1.83)	(1.72-1.70)	(1.73-1.71)
Space group	C 1 2 1	C 1 2 1	C 1 2 1
Unit cell: a, b, c (Å)	100.1, 32.7, 72.3	99.6, 32.5, 71.9	100.3, 32.8, 72.7
α, β, γ (°)	90.0, 90.4, 90.0	90.0, 90.1, 90.0	90.0, 90.6, 90.0
Total reflections	70228 (1203)	74913 (393)	98203 (408)
Unique reflections	19258 (400)	22961 (270)	22887 (277)
Multiplicity	3.6 (3.0)	3.3 (1.5)	4.3 (1.5)
Completeness (%)	89.87 (43.77)	85.66 (17.53)	80.00 (16.32)
Mean $I/\sigma(I)$	11.95 (2.43)	15.76 (2.52)	13.01 (2.38)
Wilson B-factor (Å ²)	20.63	18.57	19.62
$R_{ m merge}$	0.06153 (0.379)	0.04228 (0.1778)	0.06403 (0.1296)
$R_{ m meas}$	0.07231 (0.4529)	0.05009 (0.2453)	0.0719 (0.1654)
R_{pim}	0.03766 (0.2445)	0.02652 (0.1678)	0.03201 (0.1003)
CC½	0.995 (0.943)	0.998 (0.943)	0.995 (0.975)
CC*	0.999 (0.985)	0.999 (0.985)	0.999 (0.994)
Reflections used in	19255 (399)	22957 (270)	22878 (277)
refinement	,		
Reflections used for R_{free}	1929 (40)	1992 (24)	2010 (21)
$R_{ m work}$	0.1774 (0.5268)	0.1675 (0.6819)	0.1825 (0.3515)
R_{free}	0.2091 (0.4982)	0.2048 (0.8760)	0.2198 (0.3611)
CCwork	0.950 (0.843)	0.950 (0.851)	0.949 (0.719)
CC_{free}	0.954 (0.736)	0.937 (0.750)	0.922 (0.673)
No. non-hydrogen atoms	2323	2409	2339
macromolecules	1889	1895	1860
ligands	230	268	248
solvent	204	246	231
Protein residues	243	242	240
RMSD bond lengths (Å)	0.005	0.006	0.008
RMSD bond angles (°)	0.76	0.83	0.98
Ramachandran favored	96.60%	97.03%	96.55%
Ramachandran allowed	3.40%	2.97%	3.45%
Ramachandran outliers	0.00%	0.00%	0.00%
Rotamer outliers (%)	0.46%	0.92%	1.40%
Clashscore	3.34	3.81	6.68
Average <i>B</i> -factor (Å ²)	29.60	25.20	30.86
macromolecules	25.08	21.47	25.94
ligands	67.27	47.72	66.82
solvent	28.92	27.56	31.86
No. TLS groups	13	5	8

^{*}Statistics for the highest-resolution shell are shown in parentheses.

TABLE S5. Completeness of resolution shells for the complex of RNase A with U>v

Resolution	Number of Reflections			Completeness	ness R factor		R factor		Completeness R factor		Compared	I/σ	$R_{ m meas}$	CC1/2	Anomal.	SigAno	Nano
Limit (Å)	Observed	Unique	Possible		observed	expected					Corr.						
5.43	2834	845	867	97.50%	4.7%	5.30%	2827	20.64	5.6%	99.2	47*	1.115	433				
3.86	5194	1428	1468	97.30%	4.2%	5.50%	5191	21.53	4.9%	99.7	11	0.727	798				
3.16	6542	1805	1871	96.50%	4.9%	5.60%	6536	20.41	5.7%	99.6	14*	0.822	895				
2.74	7701	2108	2193	96.10%	6.1%	6.10%	7692	17.78	7.1%	99.4	34*	0.992	935				
2.45	8726	2363	2476	95.40%	7.0%	6.90%	8720	15.79	8.3%	99.3	45*	1.064	972				
2.24	9708	2592	2741	94.60%	8.1%	8.20%	9706	13.79	9.5%	99.2	43*	0.974	977				
2.07	10358	2748	2933	93.7%	10.50%	10.6%	10354	11.51	12.3%	98.7	30*	0.91	944				
1.94	11008	2905	3144	92.4%	17.30%	18.9%	11001	7.56	20.2%	97.4	17*	0.758	937				
1.83	8153	2463	3375	73.0%	29.90%	39.20%	7938	3.75	35.4%	94.6	11	0.587	484				
Total	70224	19257	21068	91.40%	6.2%	6.9%	69965	13.42	7.2%	99.5	30*	0.890	7375				

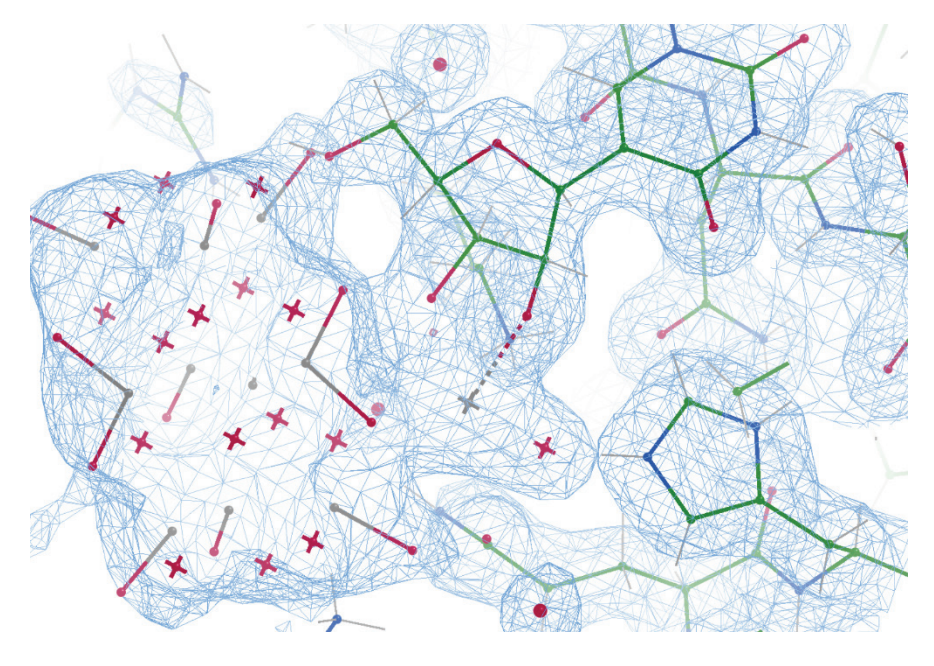
TABLE S6. Completeness of resolution shells for the complex of RNase A with $\Psi > v$

Resolution	Number of Reflections			Completeness	R factor		Completeness R factor		Compared	I/σ	$R_{ m meas}$	CC _{1/2}	Anomal.	SigAno	Nano
Limit (Å)	Observed	Unique	Possible		observed	expected					Corr.				
5.06	3560	1043	1059	98.50%	4.1%	5.10%	3556	22.97	4.9%	99.7	44*	0.966	549		
3.59	6400	1767	1791	98.70%	3.2%	5.30%	6398	23.81	3.7%	99.8	10	0.618	963		
2.94	8124	2260	2286	98.90%	3.8%	5.30%	8120	23.03	4.5%	99.7	19*	0.787	1097		
2.54	9467	2660	2703	98.40%	4.7%	5.30%	9465	21.86	5.6%	99.6	32*	0.962	1178		
2.28	10667	3005	3045	98.70%	5.1%	5.5%	10665	20.50	6.0%	99.5	36*	1.033	1264		
2.08	11719	3310	3348	98.90%	5.1%	5.7%	11718	19.16	6.1%	99.5	29*	0.951	1333		
1.92	12554	3594	3623	99.20%	6.7%	6.5%	12551	16.14	7.9%	99.2	7	0.858	1396		
1.80	8585	3353	3890	86.20%	8.7%	8.20%	8394	10	11.1%	98.6	-9	0.706	466		
1.70	3837	1969	4153	47.4%	12.90%	15.90%	3484	4.85	17.6%	97.0	-33	0.413	57		
Total	74913	22961	25898	88.70%	4.2%	5.4%	74351	17.52	5.0%	99.8	23*	0.873	8303		

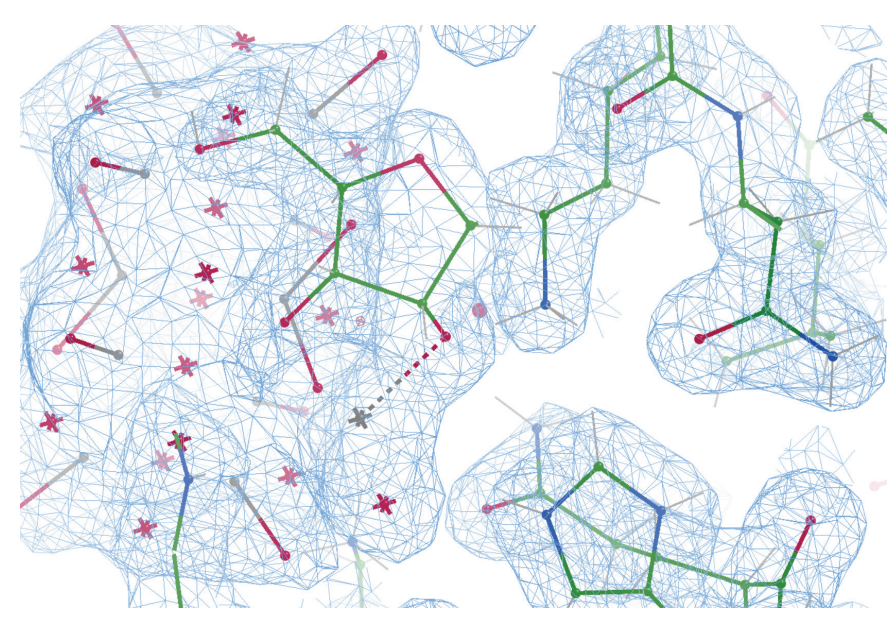
TABLE S7. Completeness of resolution shells for the complex of RNase A with $m^1\Psi > v$

Resolution	Number of Reflections			Completeness	R factor		Completeness R factor		Compared	I/σ	$R_{ m meas}$	$CC_{1/2}$	Anomal.	SigAno	Nano
Limit (Å)	Observed	Unique	Possible		observed	expected					Corr.				
5.08	3622	1035	1067	97.00%	5.5%	6.90%	3612	17.39	6.5%	99.4	24*	0.868	433		
3.61	6462	1750	1804	97.00%	5.2%	7.00%	6454	17.98	6.1%	99.4	1	0.666	798		
2.95	8204	2246	2317	96.90%	5.9%	7.00%	8200	17.18	6.9%	99.2	3	0.759	895		
2.55	9059	2582	2733	94.50%	6.7%	7.10%	9044	16.02	8.0%	98.9	11*	0.860	935		
2.29	9454	2803	3057	91.70%	7.0%	7.30%	9323	14.62	8.4%	98.8	15*	0.897	972		
2.09	9768	2975	3399	87.50%	7.4%	7.70%	9565	13.24	8.9%	99.0	3	0.808	977		
1.93	9964	3096	3649	84.80%	9.1%	8.90%	9757	10.67	10.9%	98.7	-15	0.700	944		
1.81	6734	2478	3923	63.2%	11.50%	11.30%	6227	6.92	14.0%	98.3	-3	0.688	937		
1.71	2836	1251	4202	29.8%	14.40%	17.50%	2427	3.89	18.0%	97.4	-19	0.501	484		
Total	66103	20216	26151	77.30%	6.1%	7.2%	64609	13.10	7.3%	99.5	5	0.777	7375		

Supplementary Information



Two **FIGURE S7.** perspectives of the $2F_{\rm o} - F_{\rm c}$ electron density maps near the vanadyl group in the crystal structure of the RNase $A \cdot m^1 \Psi > v$ complex. Vanadium atoms depicted in grey, oxygen atoms in pink, carbon atoms in green, and nitrogen atoms in blue. The vanadyl group adopts a tetrahedral geometry that includes the 2' and 3' oxygens of ribose, an oxygen in a proximal decavanadate, and nonbridging oxygen. The image is depicted at a contour level of 1.0σ .



9. Decavanadates in Crystal Structures

Decayanadate was found in A each crystal structure (Fig. S8). That is not surprising per se because the crystals were grown at pH 5.5, where decavanadates are a predominant species (Aureliano et al. 2022), and because decavanadate is known to bind to RNase A and Raines (Messmore 2000). A previous X-ray crystallographic study of RNase A·U>v did not report presence the of decavanadate (Ladner et al. 1997), though the mother liquor therein contained a high concentration of 2methyl-2-propanol, which can precipitate vanadate.

In addition, the electron density of the vanadyl group c in each complex was in a tetrahedral conformation (Fig. S7) and appeared to be a complex with a proximal decavanadate. These interactions had no impact on nucleobase binding in the active site (Fig. 3). To the extent of our knowledge this vanadate species (decavanadate in complex with an additional oxidovanadate) has not been reported previously as a stable species at this pH and could be stabilized by the enzymic active site.

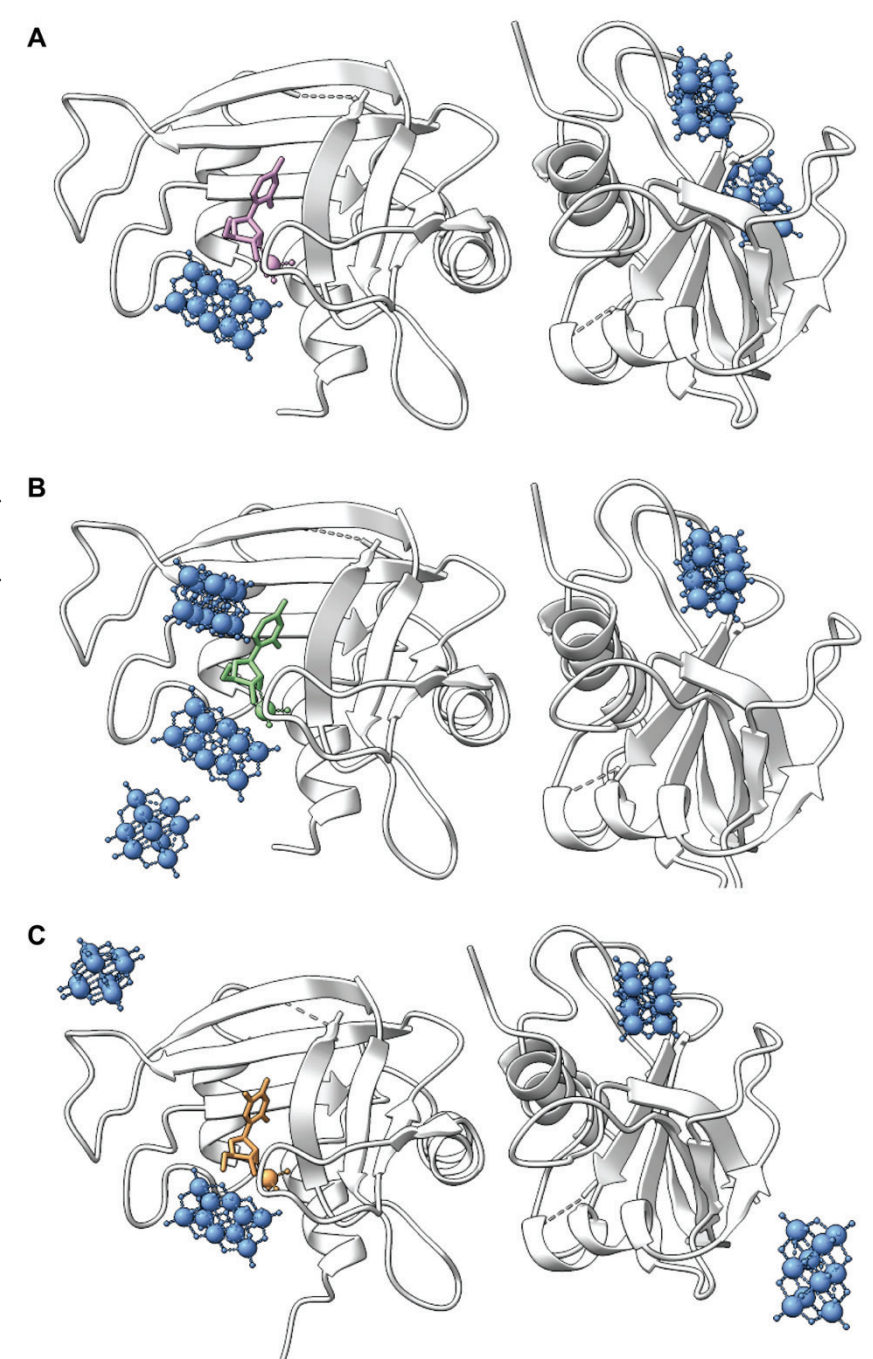


FIGURE S8. Vanadium in the asymmetric units of (A) U>v, (B) Ψ >v, and (C) m¹ Ψ >v. Nucleoside 2',3'-cyclic vanadate complexes are in only one monomer of the unit cell whereas decavanadates exist in different regions around the two monomers.

10. Computational Analyses

10.1. Top-Ranked Docking Poses of Enzyme-Substrate Complexes

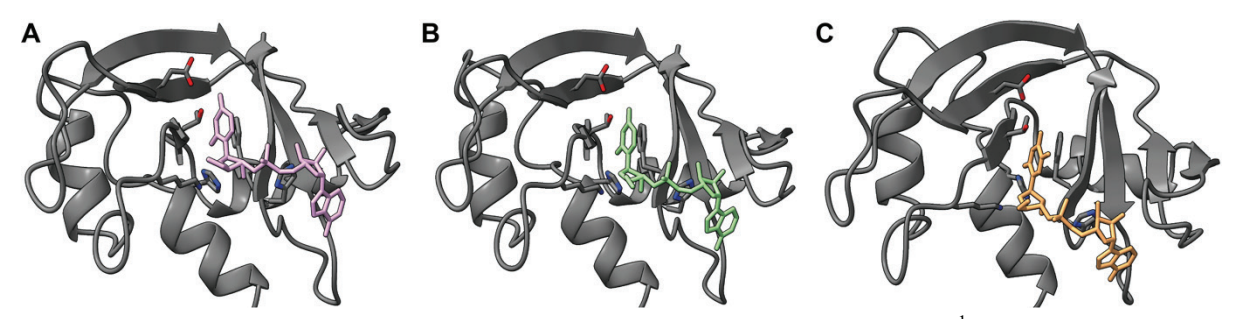


FIGURE S9. Top-ranked docking poses of UpA (A, pink), ΨpA (B, green) and $m^1 \Psi pA$ (C, orange) bound to RNase A (gray).

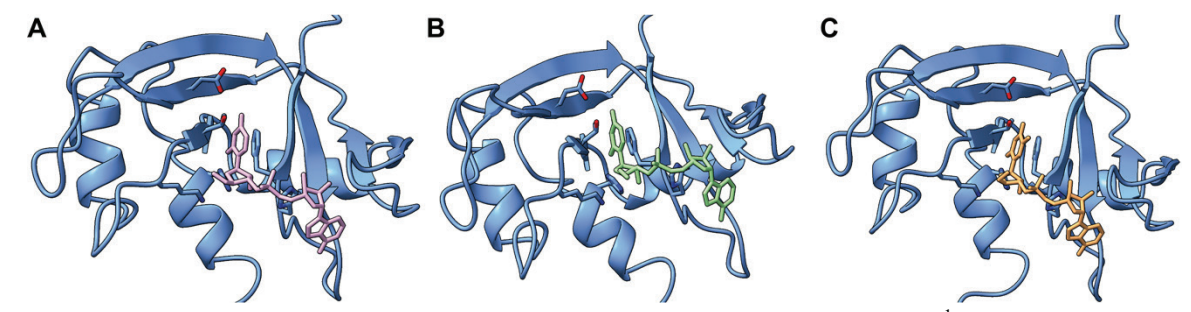


FIGURE S10. Top-ranked docking poses of UpA (A, pink), Ψ pA (B, green) and $m^1\Psi$ pA (C, orange) bound to RNase 1 (blue).

10.2. Molecular Dynamics Simulations of RNase A. Substrate Complexes

MD simulations for each substrate were initiated from the RNase A substrate complexes obtained from molecular docking studies (Fig. S9) and were performed for 1500 ns. We used the TIP3P water model along with the ff14SB and gaff parameter sets for the protein and ligands, respectively. For each simulation, an average structure was generated using 7500 frames from the final 750 ns of the simulation.

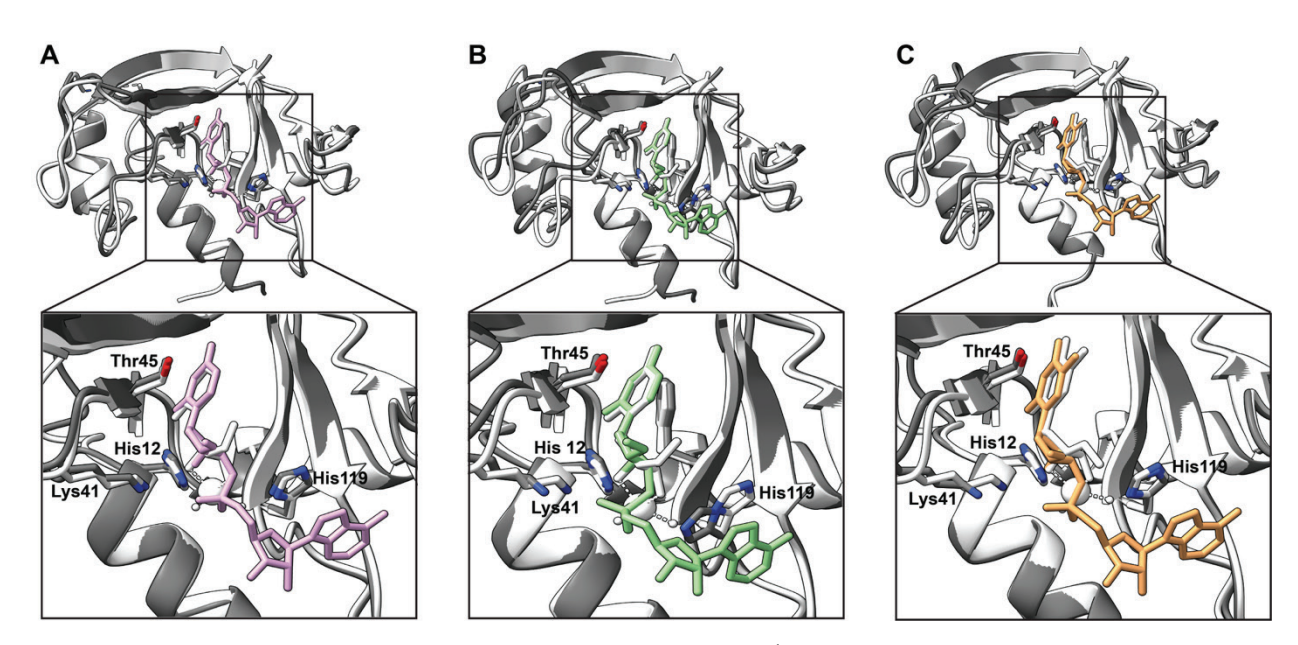


FIGURE S11. Overlay of UpA (A, pink), Ψ pA (B, green) and $m^1\Psi$ pA (C, orange) bound to RNase A (gray) obtained from MD simulations with the crystal structures of U>v (A, white), Ψ >v (B, white), and $m^1\Psi$ >v (C, white) bound to RNase A (white).

10.3. Molecular Dynamics Simulations of RNase 1. Substrate Complexes

MD simulations for each substrate were initiated from the RNase 1·substrate complexes resulting from molecular docking studies (Fig. S10) and were performed for 750 ns. We used the TIP3P water model and the ff14SB parameter set for the protein. For the ligands, the RNA force field OL3 and modrna08 parameters were applied to natural and modified dinucleotides, respectively. For each simulation, an average structure was generated using 7500 frames.

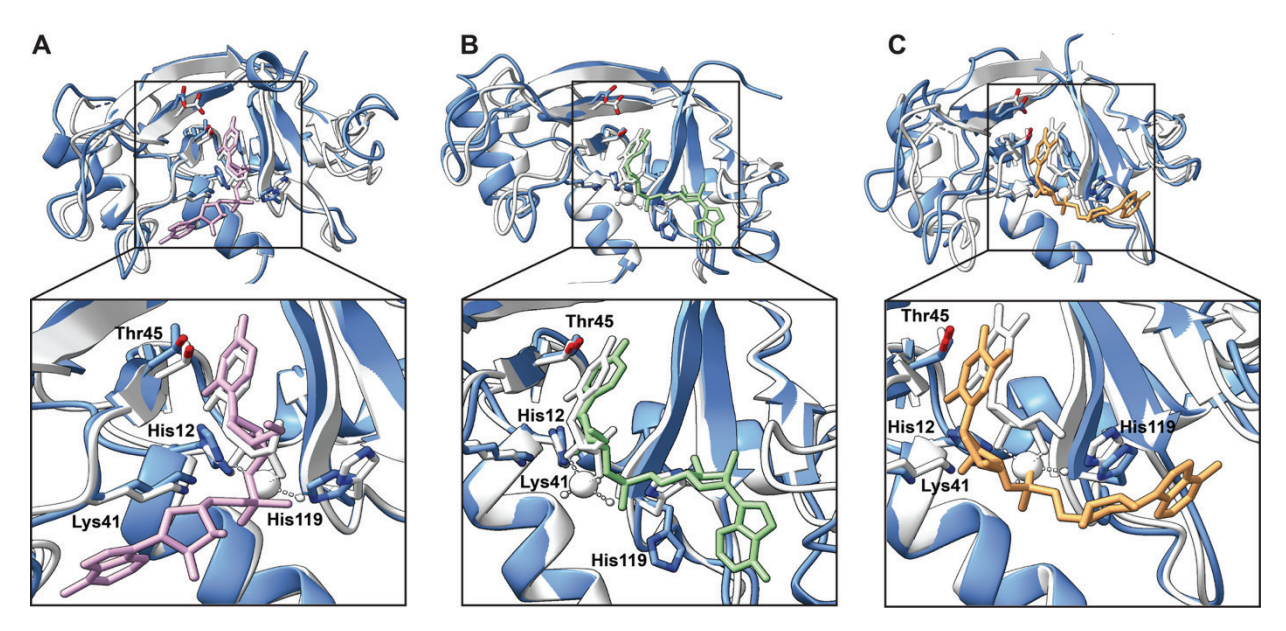


FIGURE S12. Overlay of UpA (A, pink), ΨpA (B, green) and $m^1 \Psi pA$ (C, orange) bound to RNase 1 (blue) obtained from MD simulations with the crystal structures of U>v (A, white), $\Psi > v$ (B, white), and $m^1 \Psi > v$ (C, white) bound to RNase A (white).

10.4. RMSD and RMSF Plots for Molecular Dynamics Simulations of RNase A and RNase 1

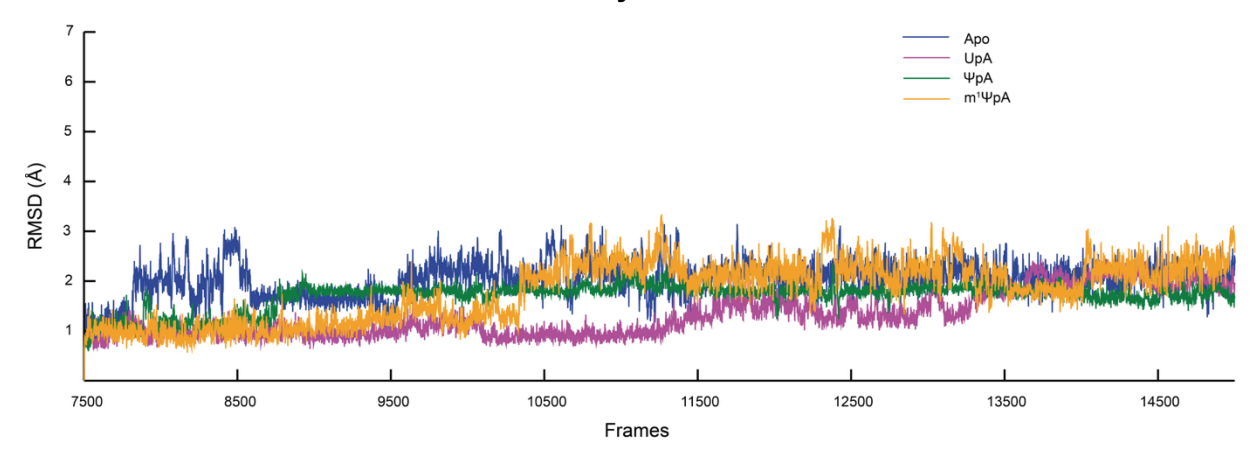


FIGURE S13. RMSD plots based on the last 750 ns of each of the four simulations of RNase A and its substrate complexes, referenced to the pre-production structures. For the simulations, the TIP3P water model was used along with the ff14SB and gaff parameter sets for the protein and ligands, respectively. The plateaued RMSDs indicate the stabilization of the protein backbone.

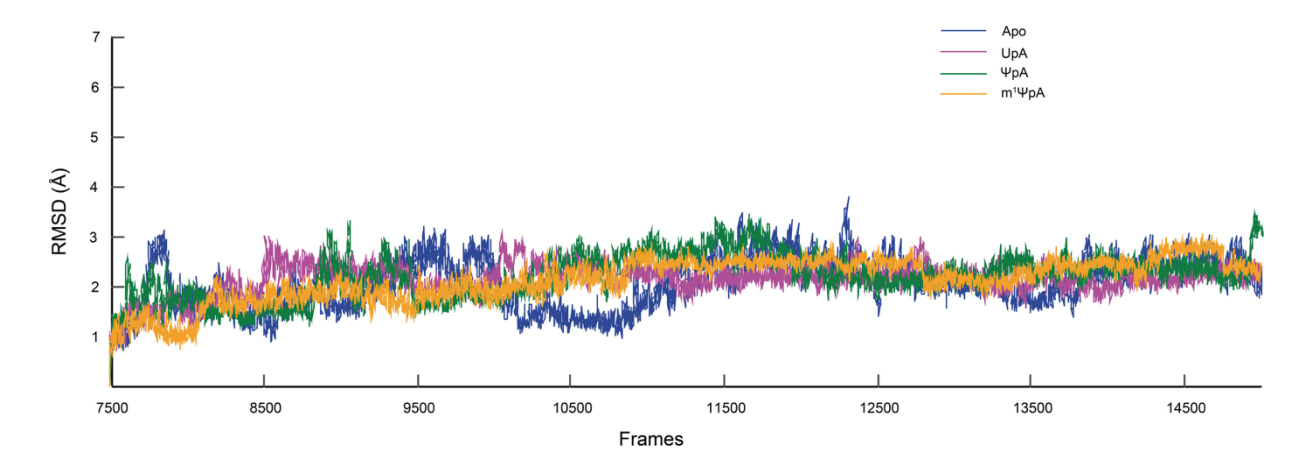


FIGURE S14. RMSD plots based on the last 750 ns of each of the four simulations of RNase 1 and its substrate complexes, referenced to the pre-production structures. For the simulations, the TIP3P water model was used along with the ff14SB and gaff parameter sets for the protein and ligands, respectively. The plateaued RMSDs indicate the stabilization of the protein backbone.

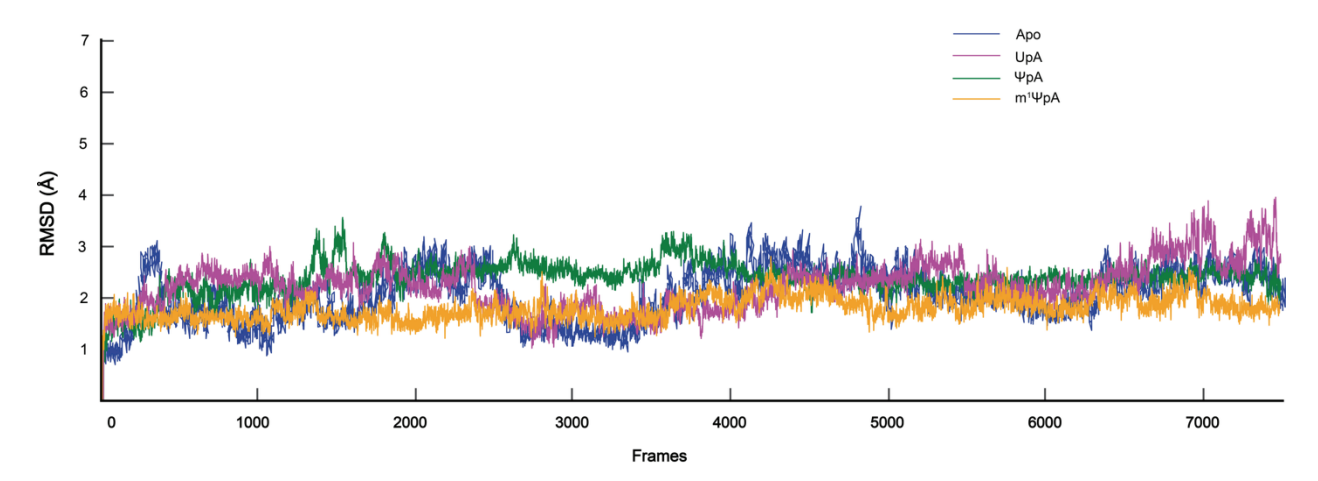


FIGURE S15. RMSD plots of each of the four 750 ns simulations of RNase 1 and its substrate complexes. For the simulations, the TIP3P water model was used along with the ff14SB parameter set for the protein. For the ligands, the RNA force field OL3 and modrna08 parameters were applied to the canonical and modified dinucleotides, respectively. The plateaued RMSDs indicate the stabilization of the protein backbone.

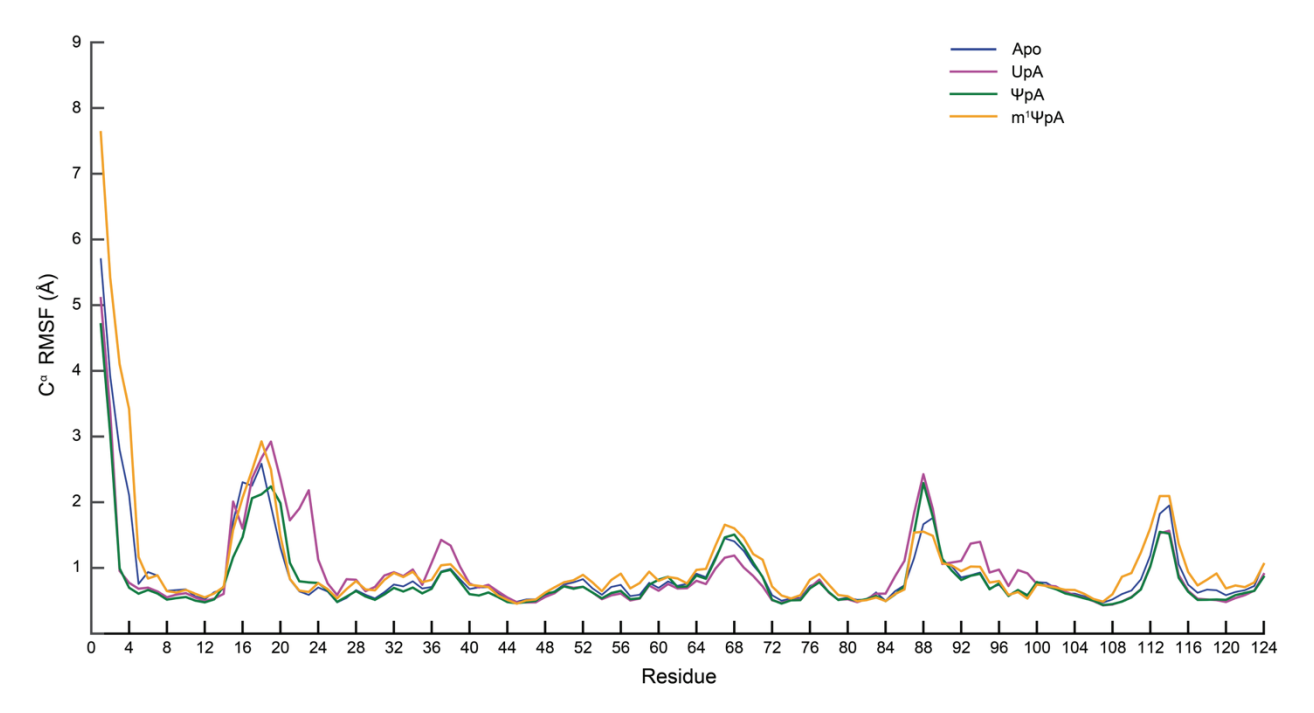


FIGURE S16. RMSF plots of C^{α} of each residue in RNase A and its substrate complexes, computed over the final 750 ns of the production-phase simulations, indicating residue-level mobility. The RMSF profiles of the four RNase A systems are similar. The regions showing larger fluctuations are distal from the key residues for catalysis (His12, Lys41, Thr45, Asp83, His119, and Phe120), which are relatively immobile.

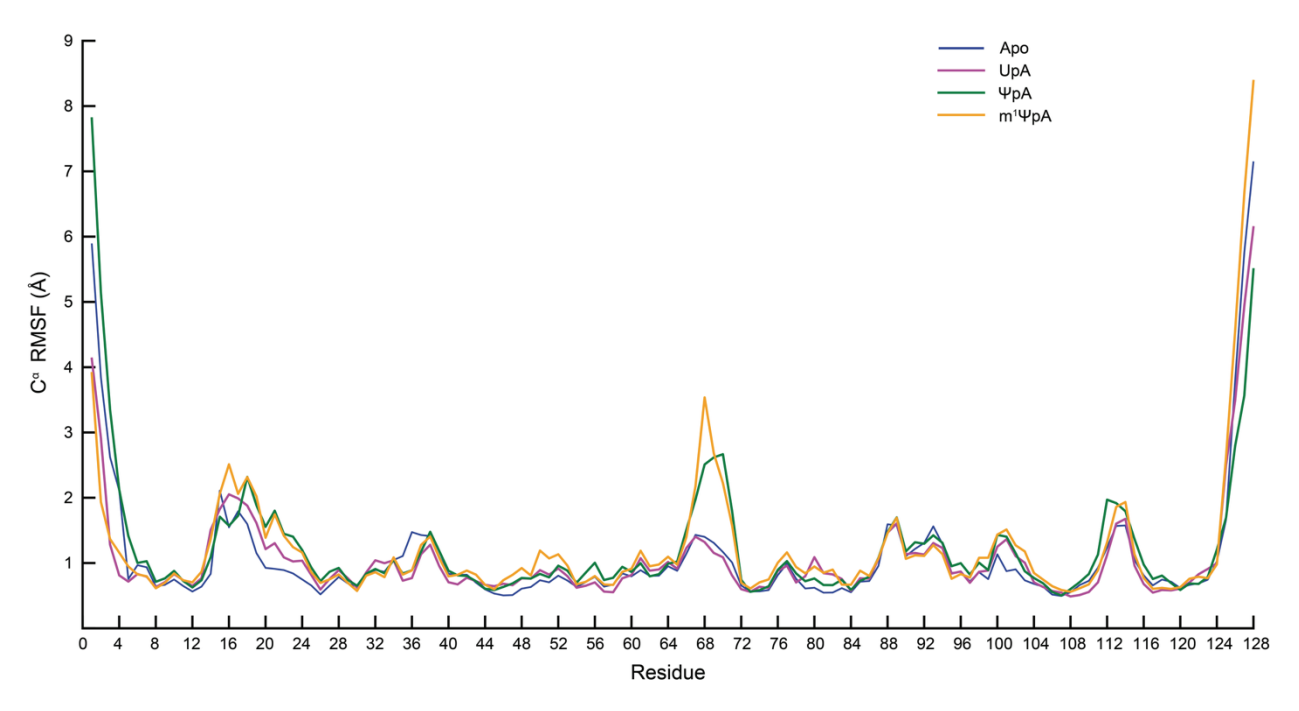


FIGURE S17. RMSF plots of C^{α} of each residue in RNase 1 and its substrate complexes, computed over the final 750 ns of the production-phase simulations, indicating residue-level mobility. As with RNase A (Fig. S16), the regions showing larger fluctuations are distal from the key residues for catalysis (His12, Lys41, Thr45, Asp83, His119, and Phe120), which are relatively immobile. Notably, the RMSF values of residues between the Cys65 and Cys72 half-cystine residues are substantially larger in the ΨpA and m¹ΨpA complexes than in the apo enzyme and UpA complex.

11. Kinetic Data for Non-Enzymatic UpA and m¹ΨpA Cleavage

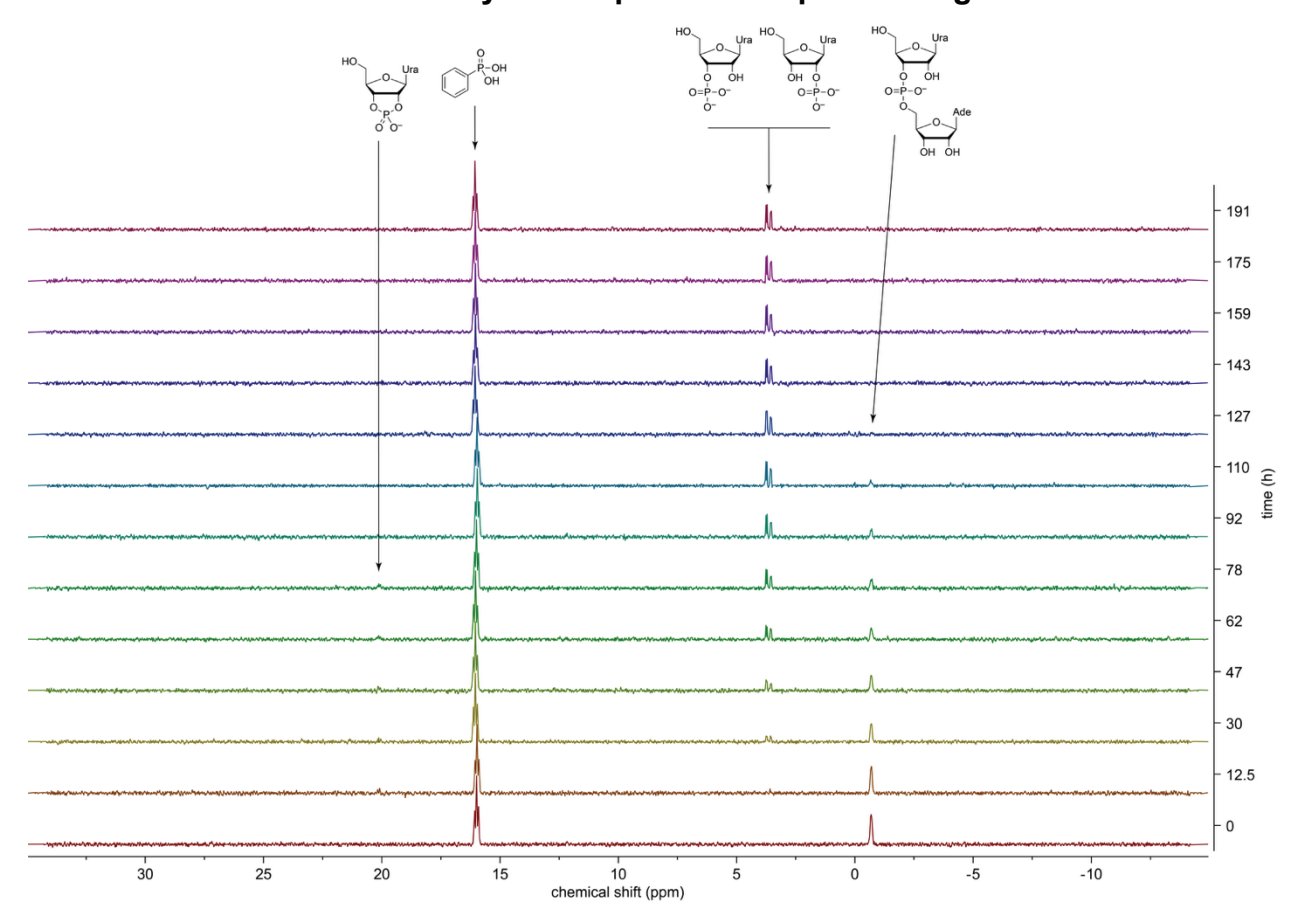


FIGURE S18. Time course of the ³¹P NMR spectra for the uncatalyzed cleavage of UpA.

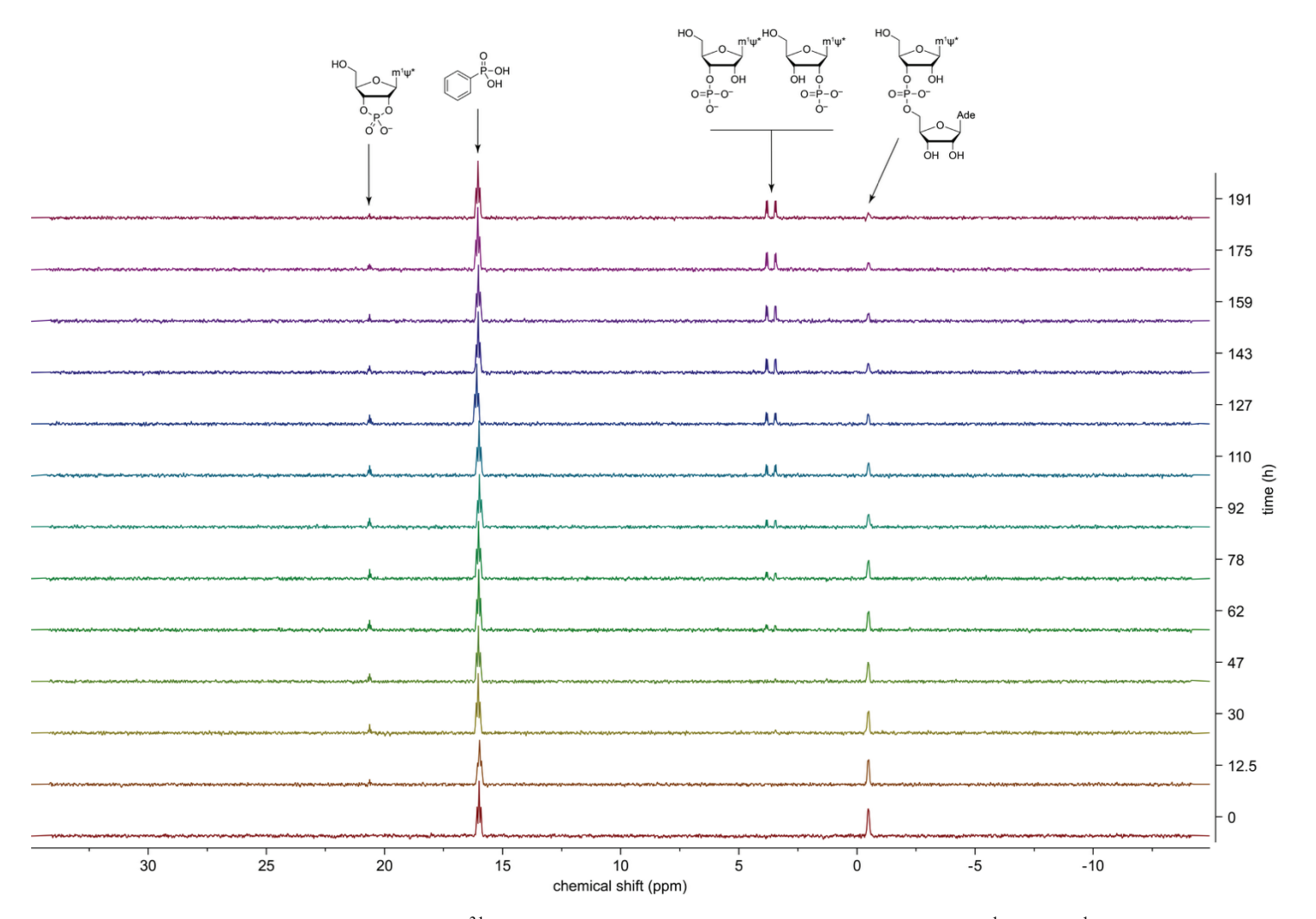
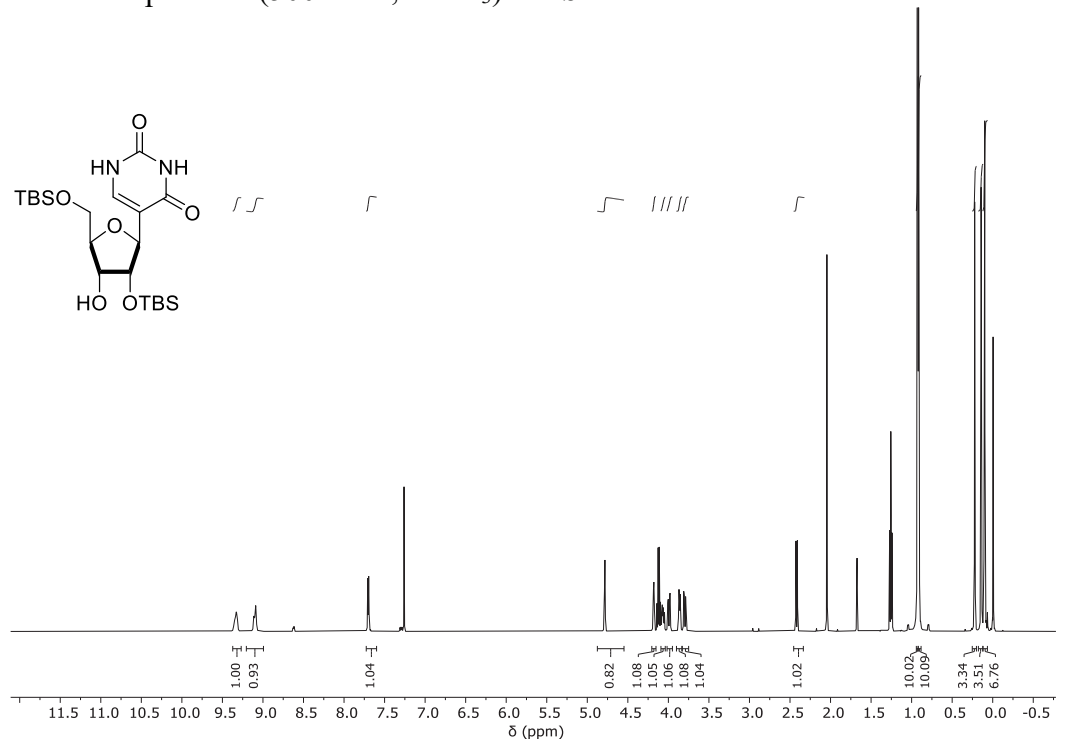
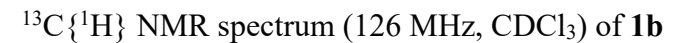


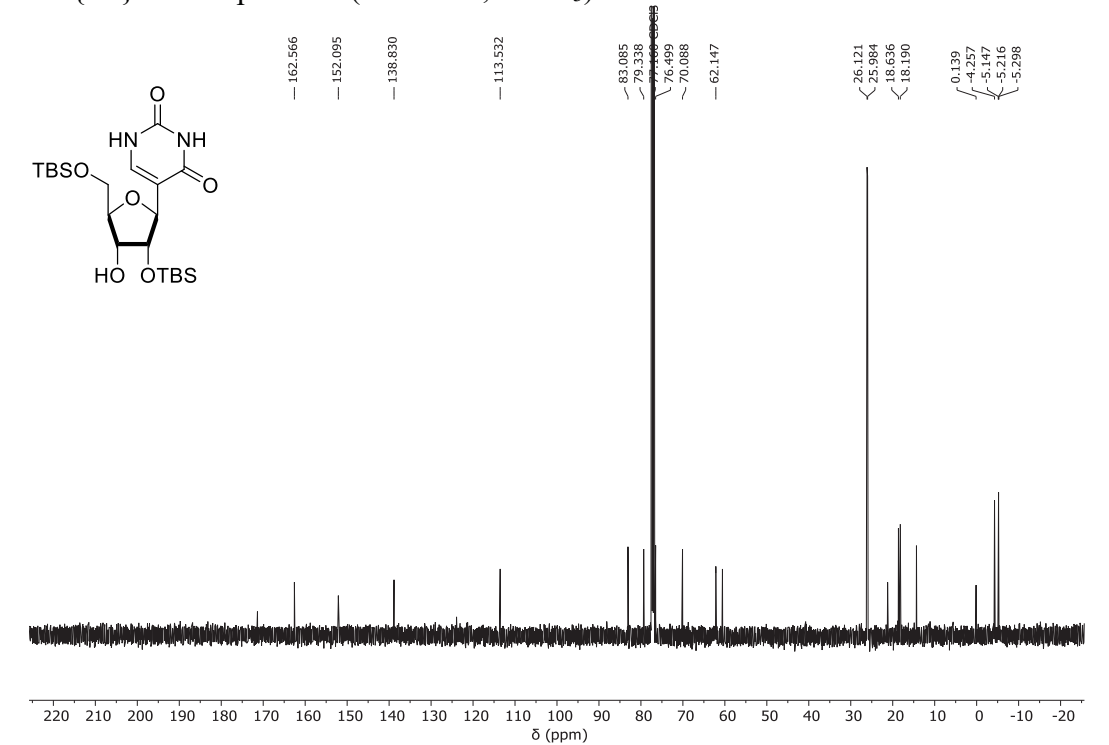
FIGURE S19. Time course of the ³¹P NMR spectra for the uncatalyzed cleavage of m¹ Ψ pA. m¹ Ψ * = N¹-methylpseudouracil nucleobase.

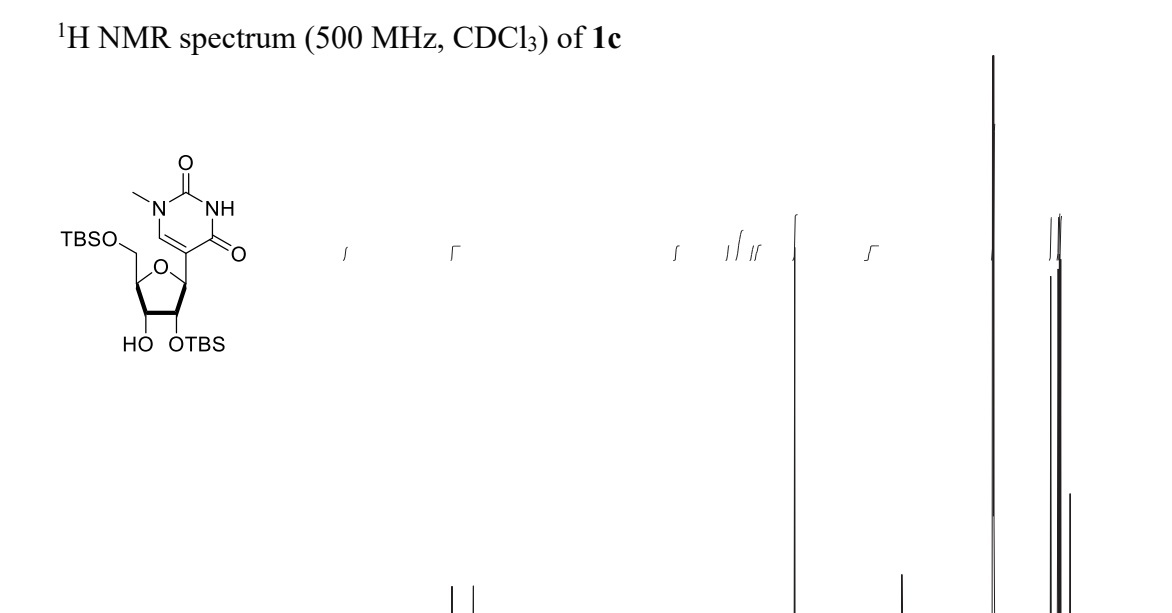
12. NMR Spectra

¹H NMR spectrum (500 MHz, CDCl₃) of **1b**

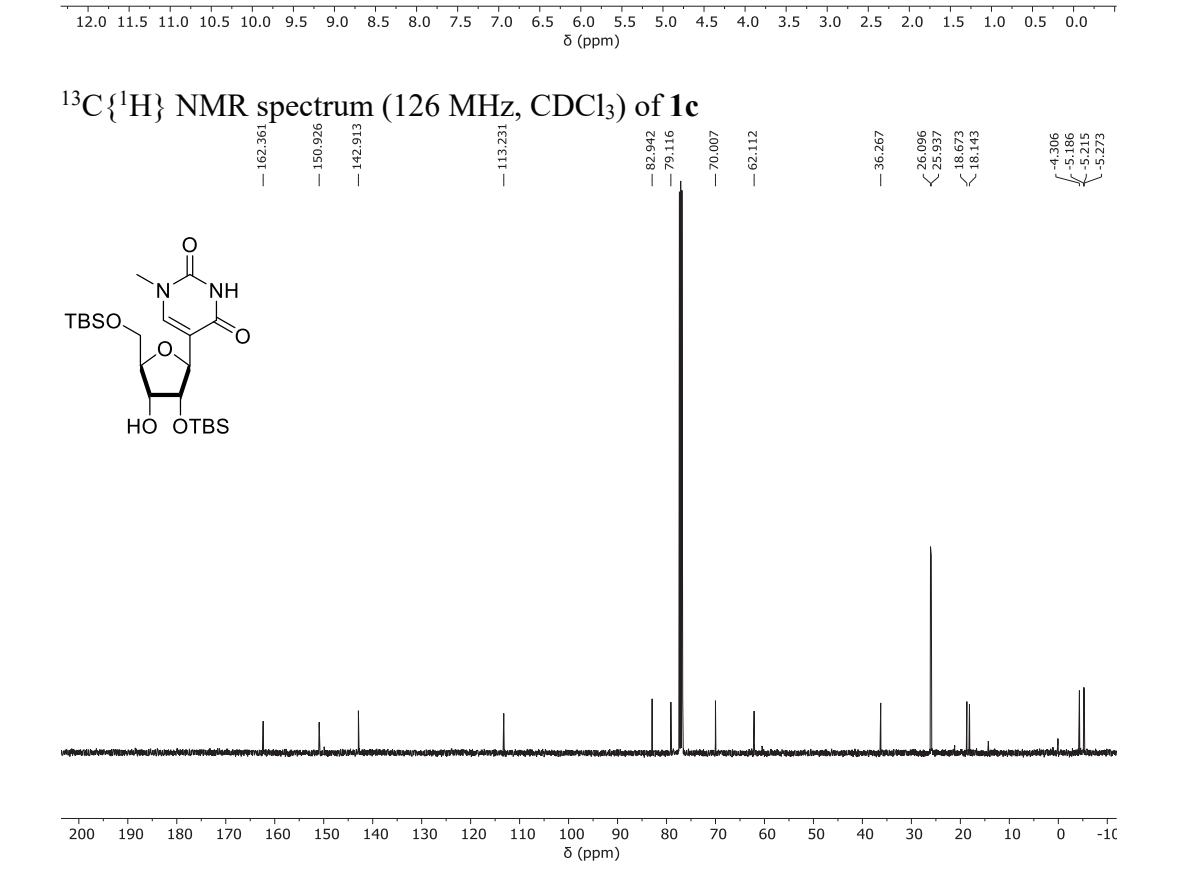


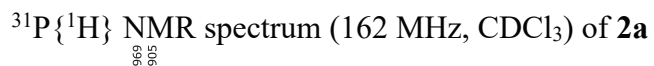


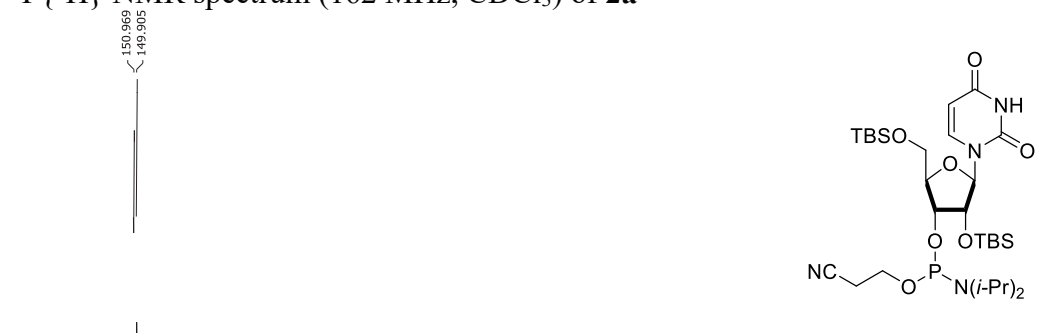




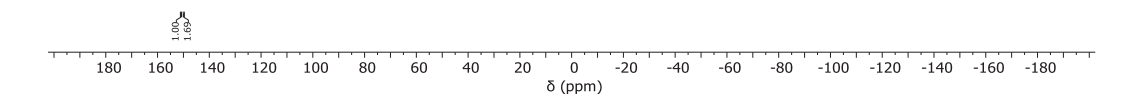
1.03 2.064 1.014 1.06 3.12=

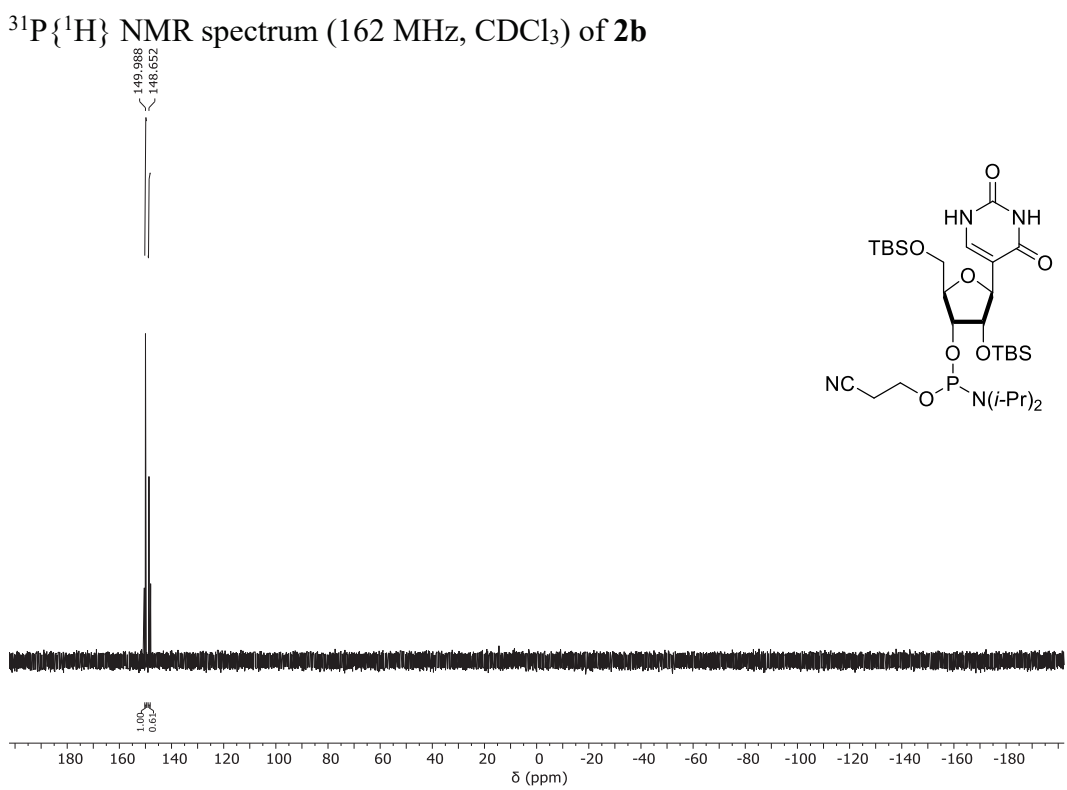


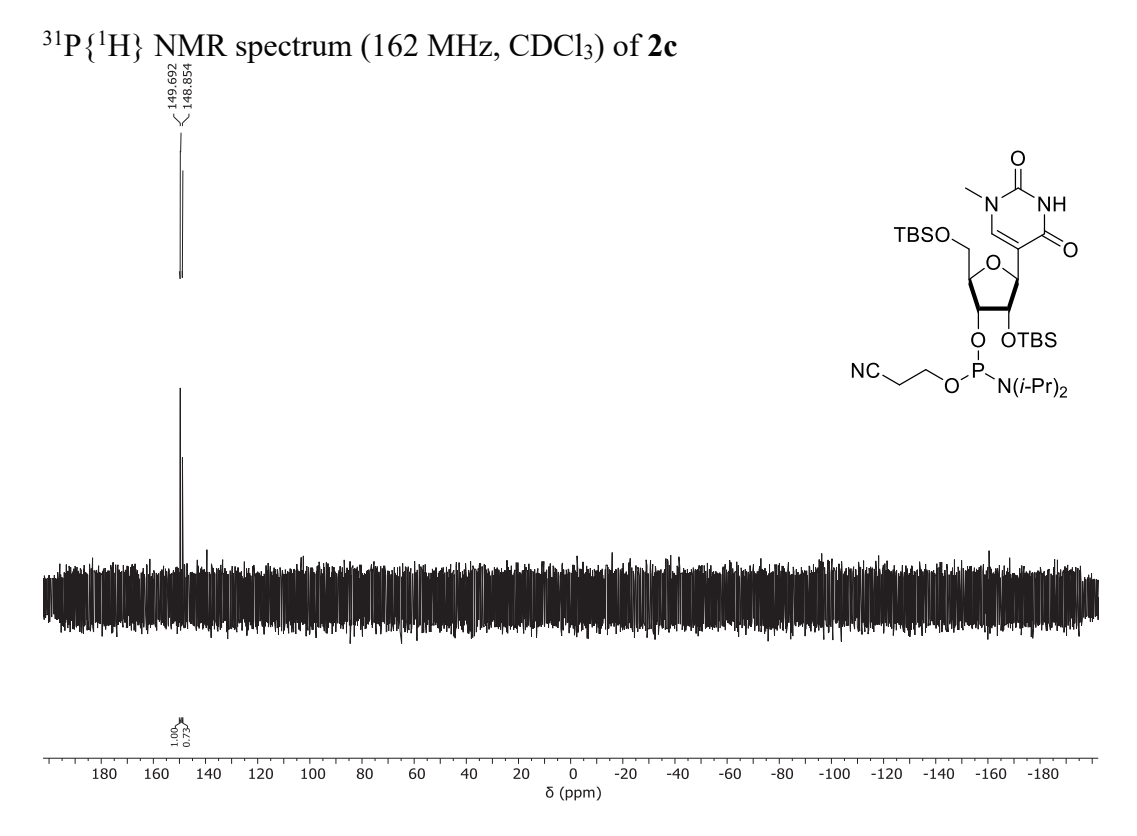


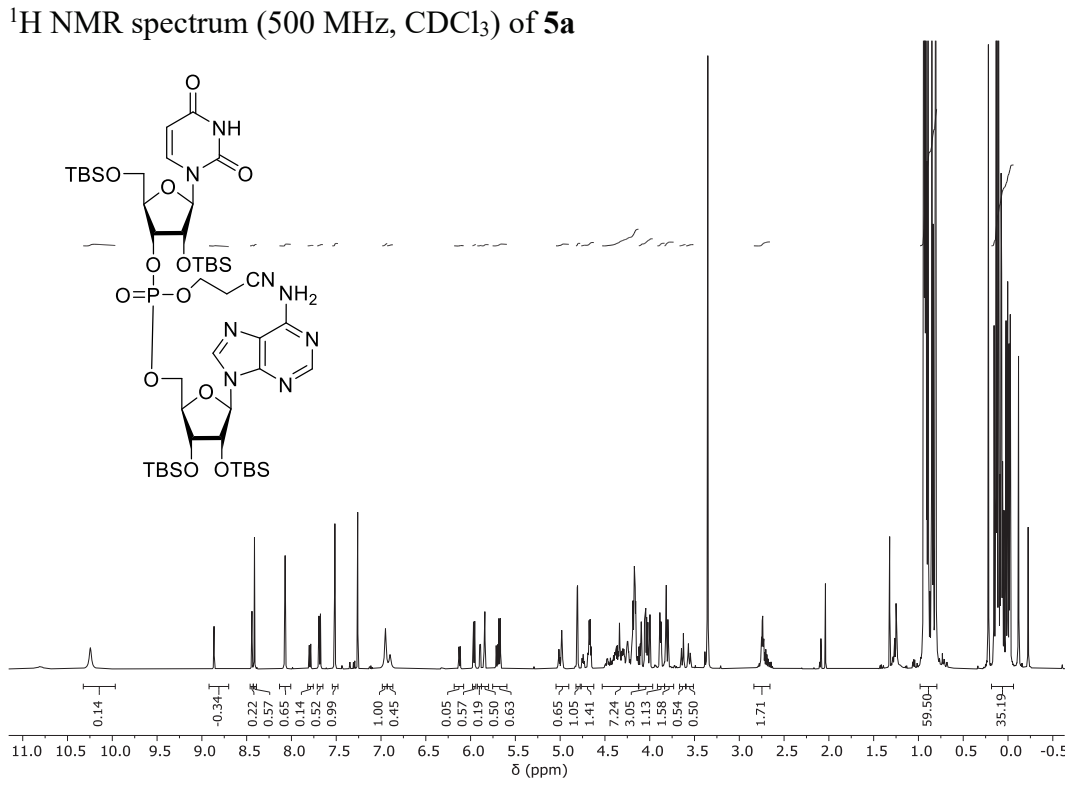


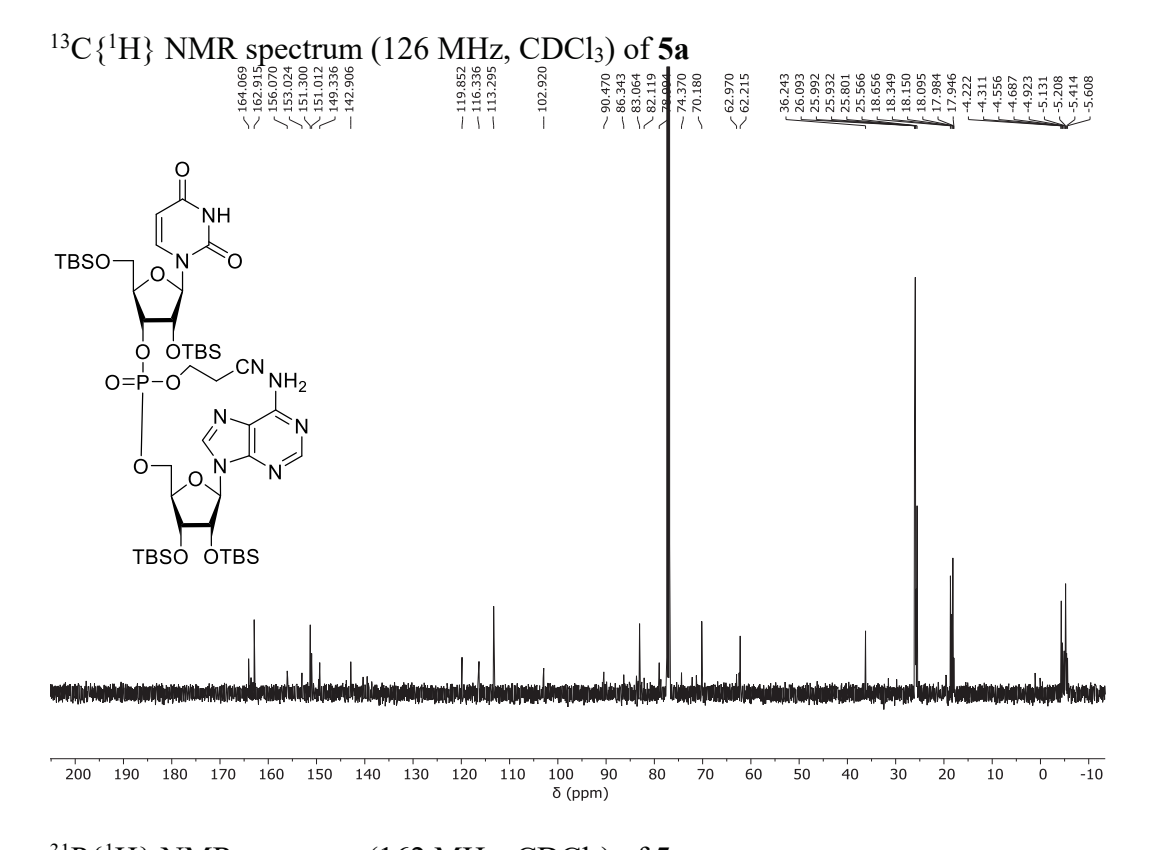


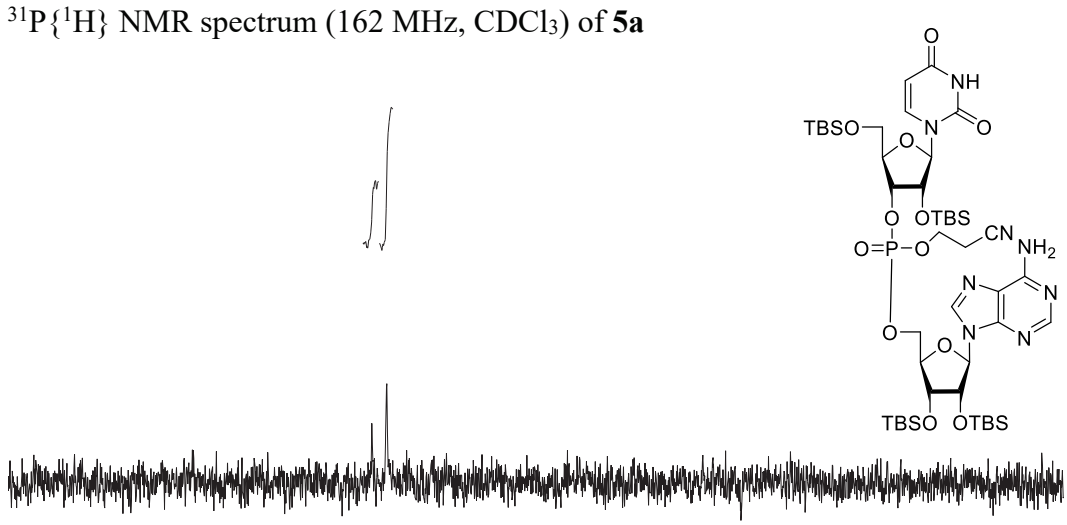


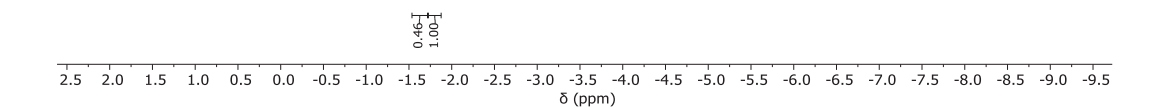


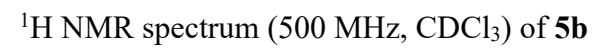


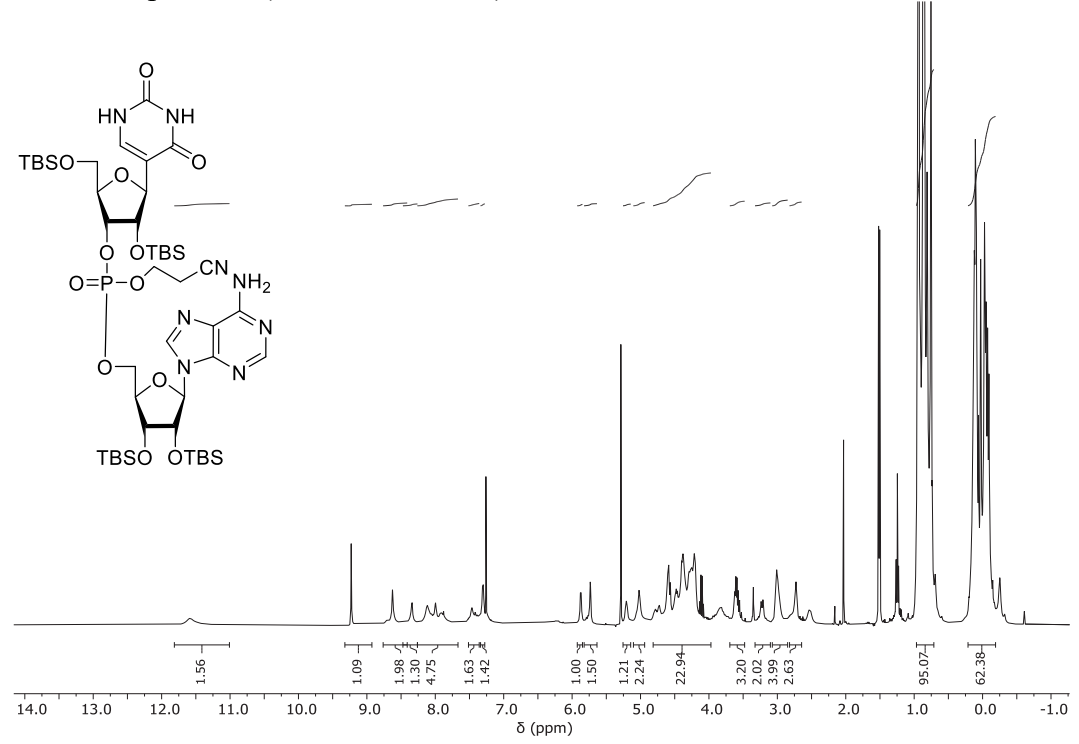


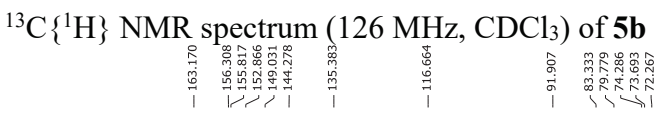


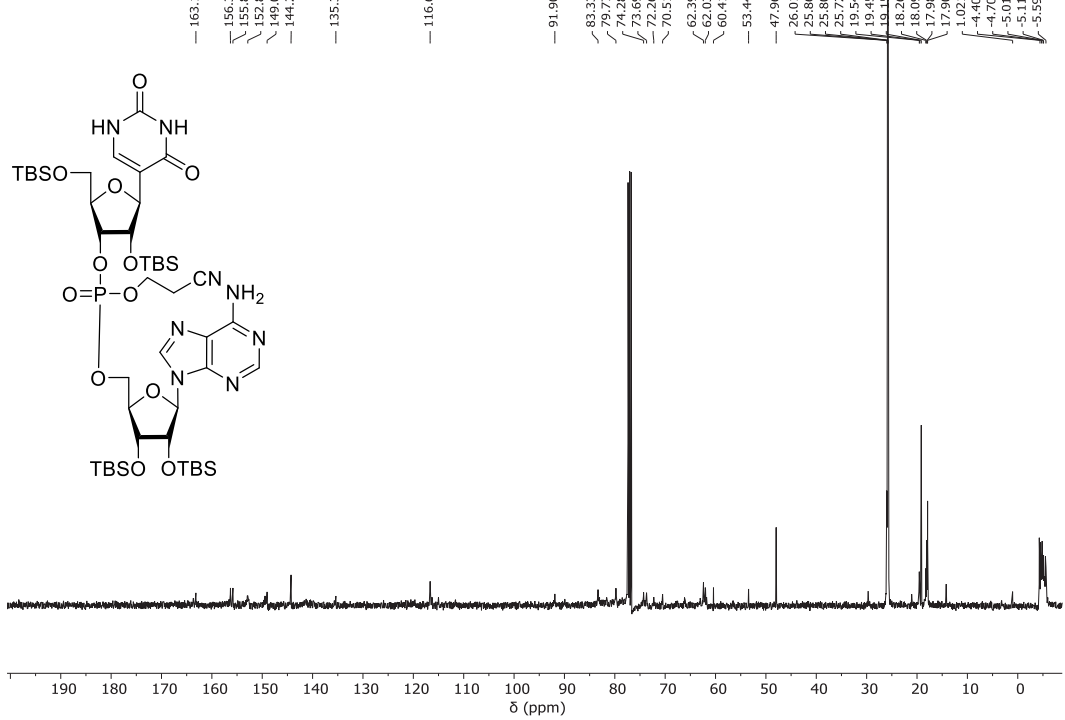


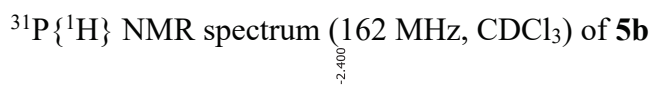


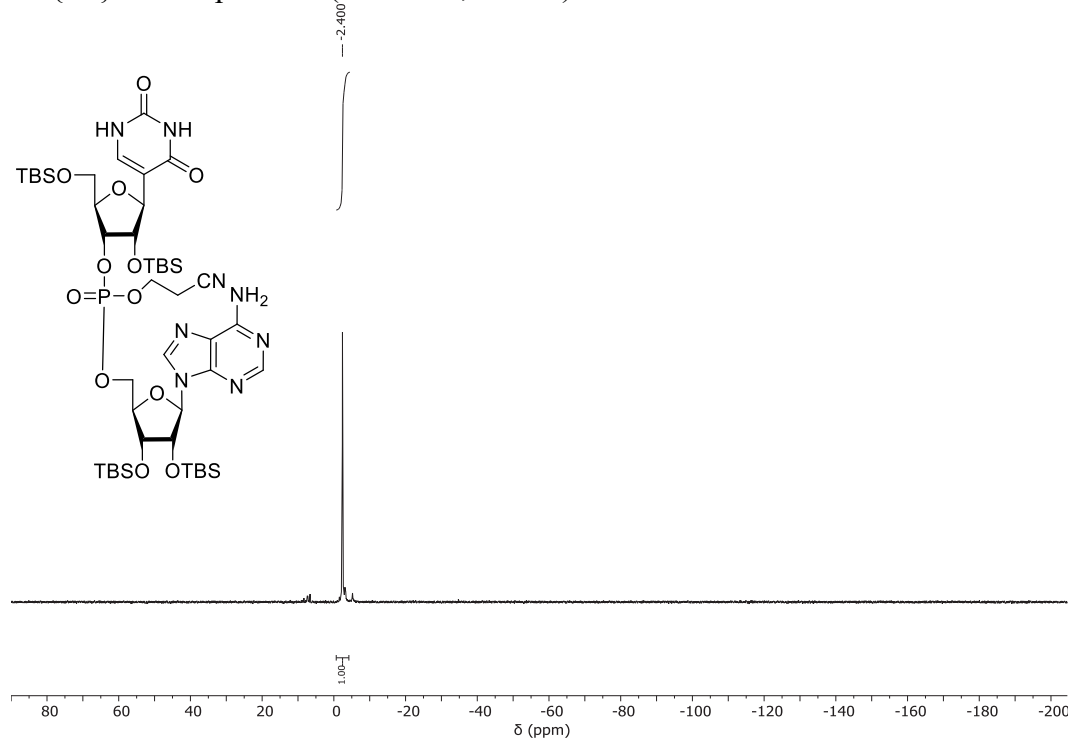




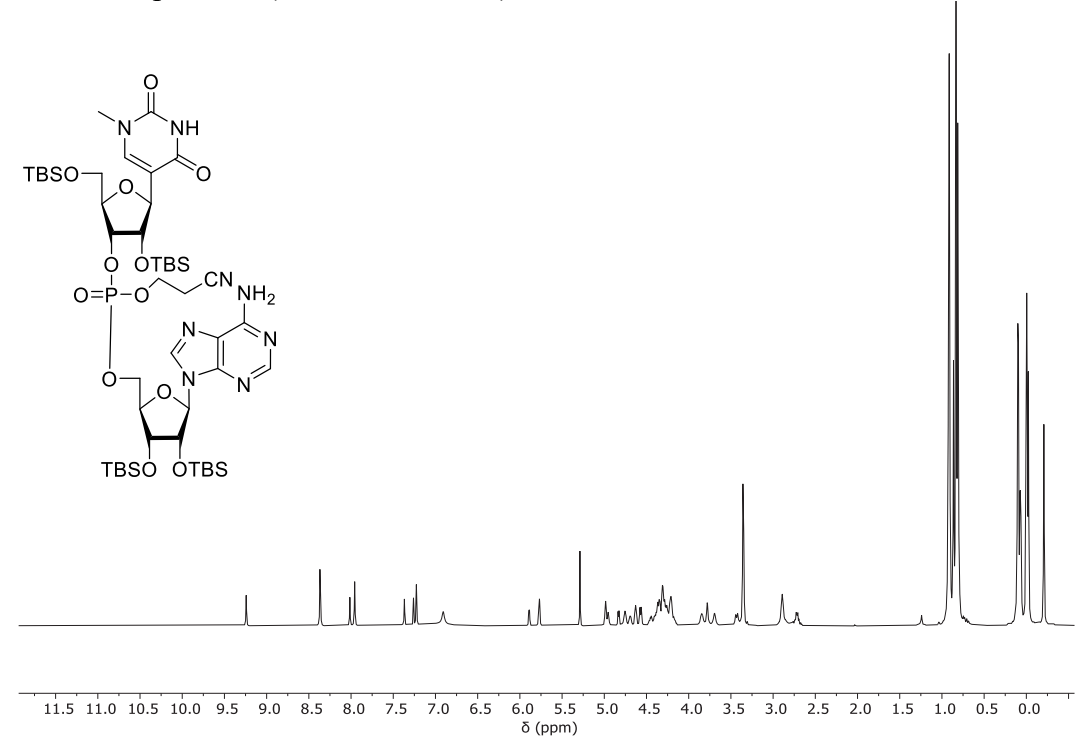


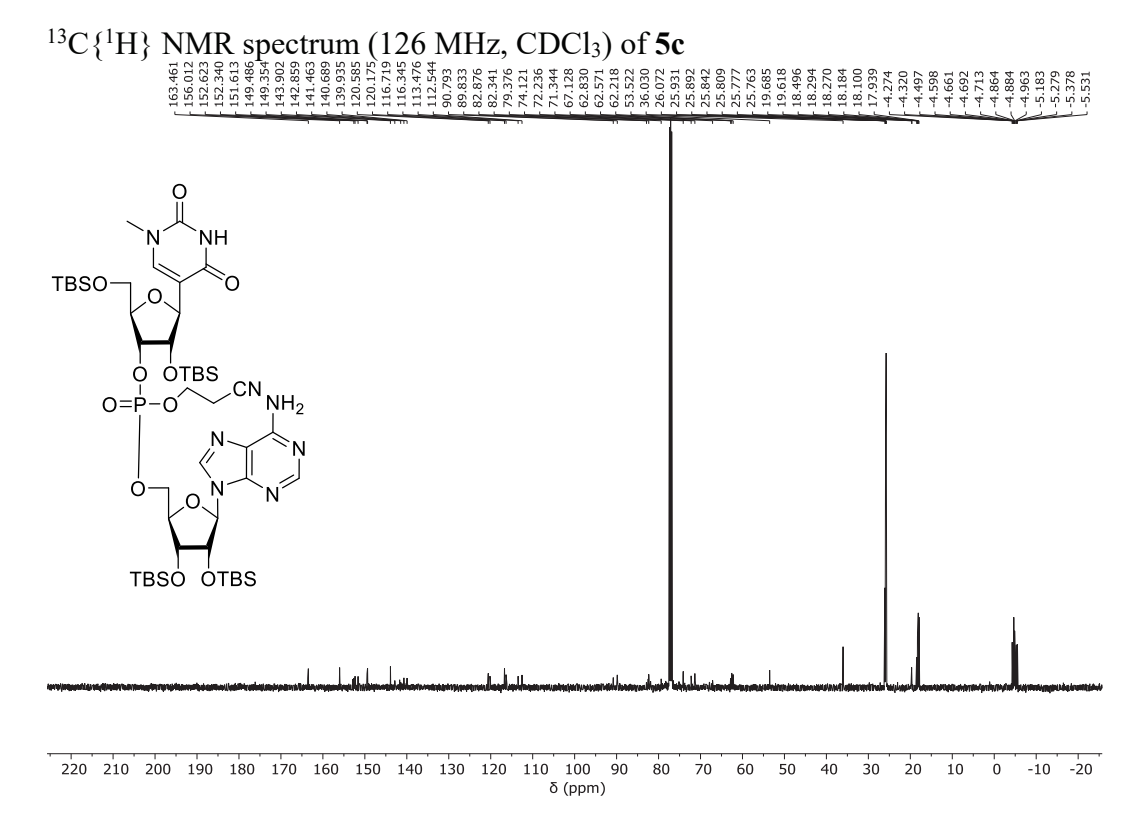


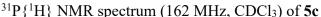


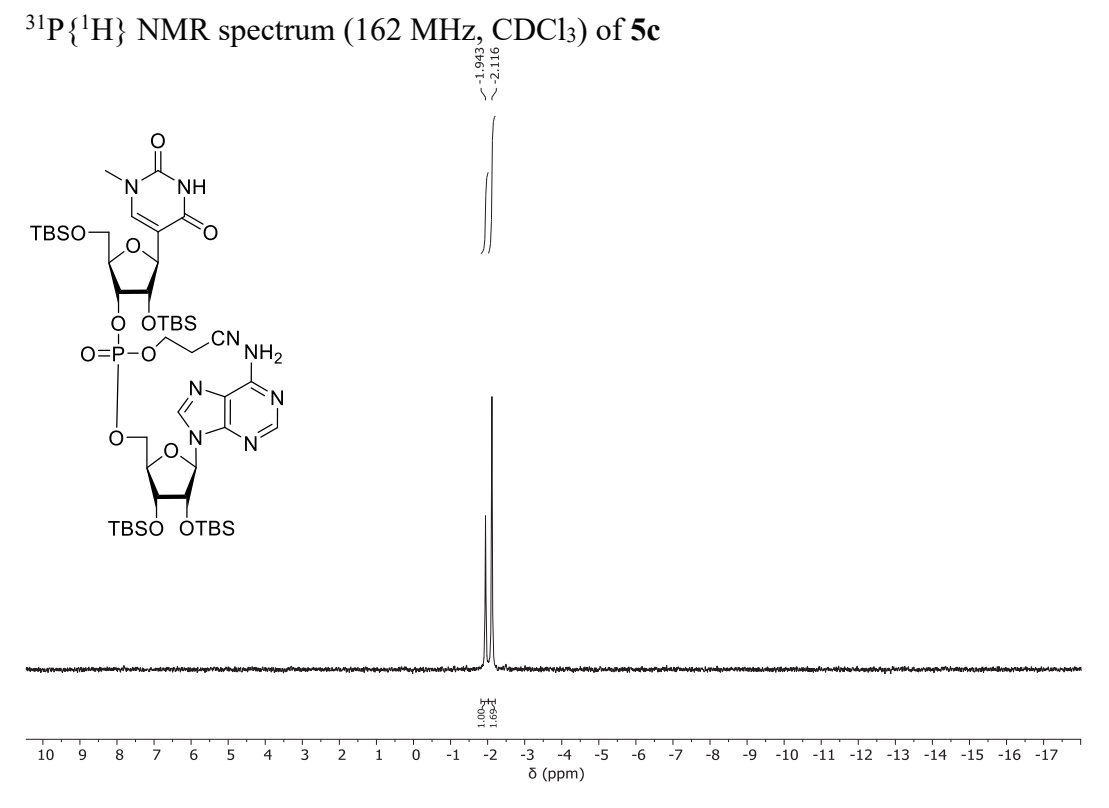


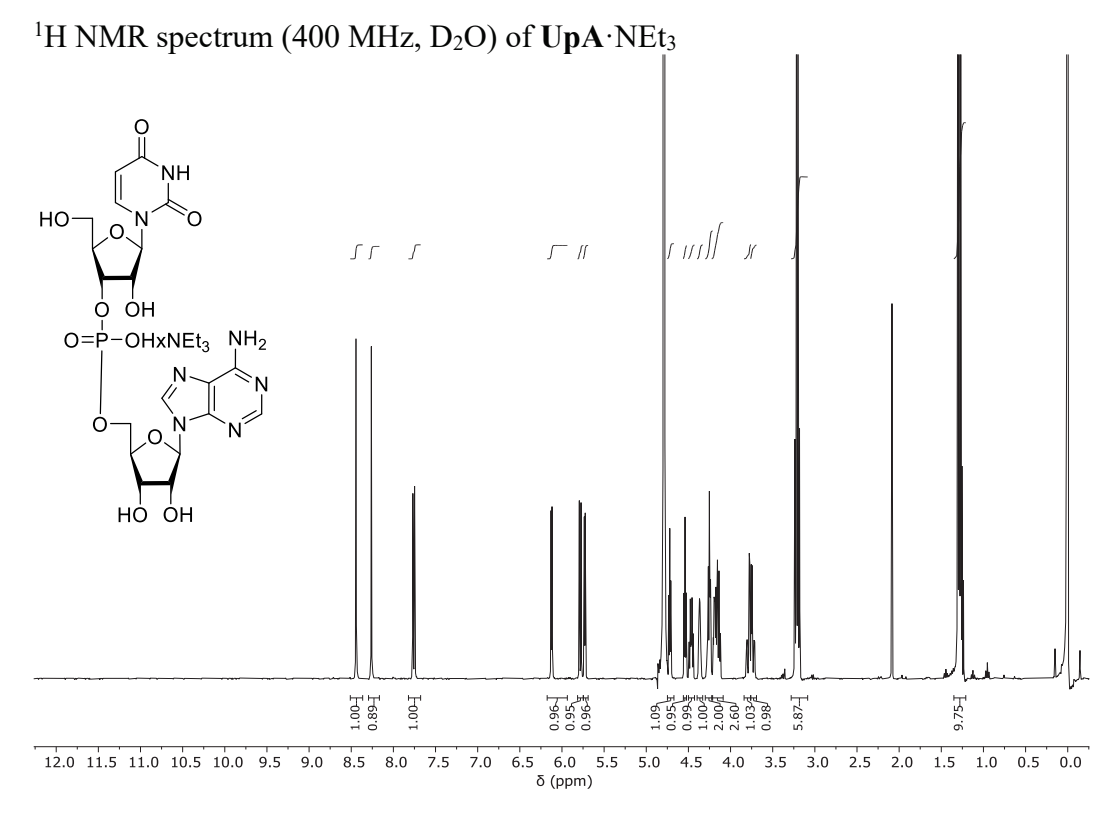
¹H NMR spectrum (500 MHz, CDCl₃) of **5c**

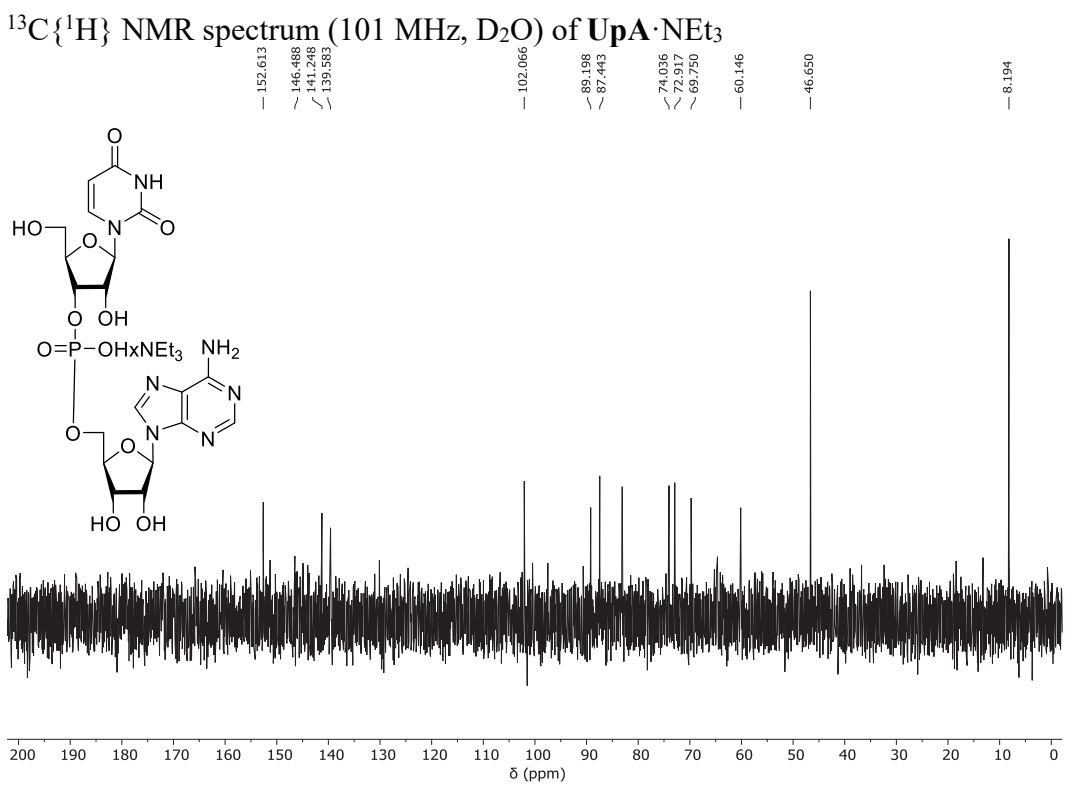




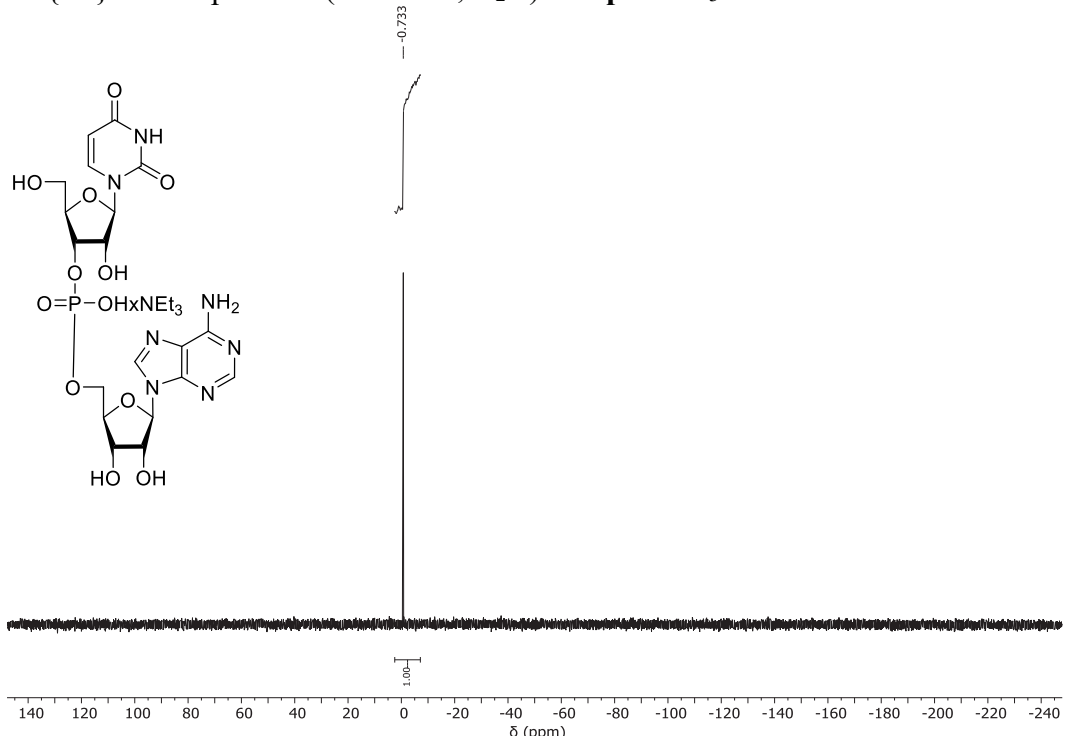




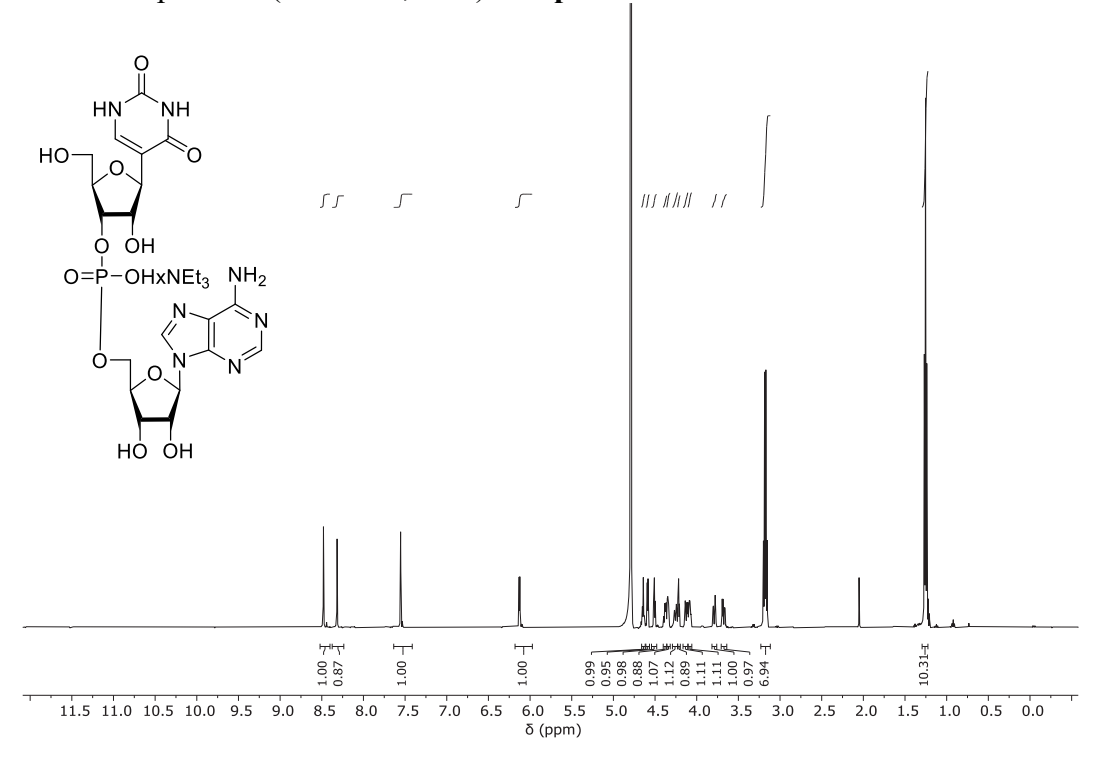


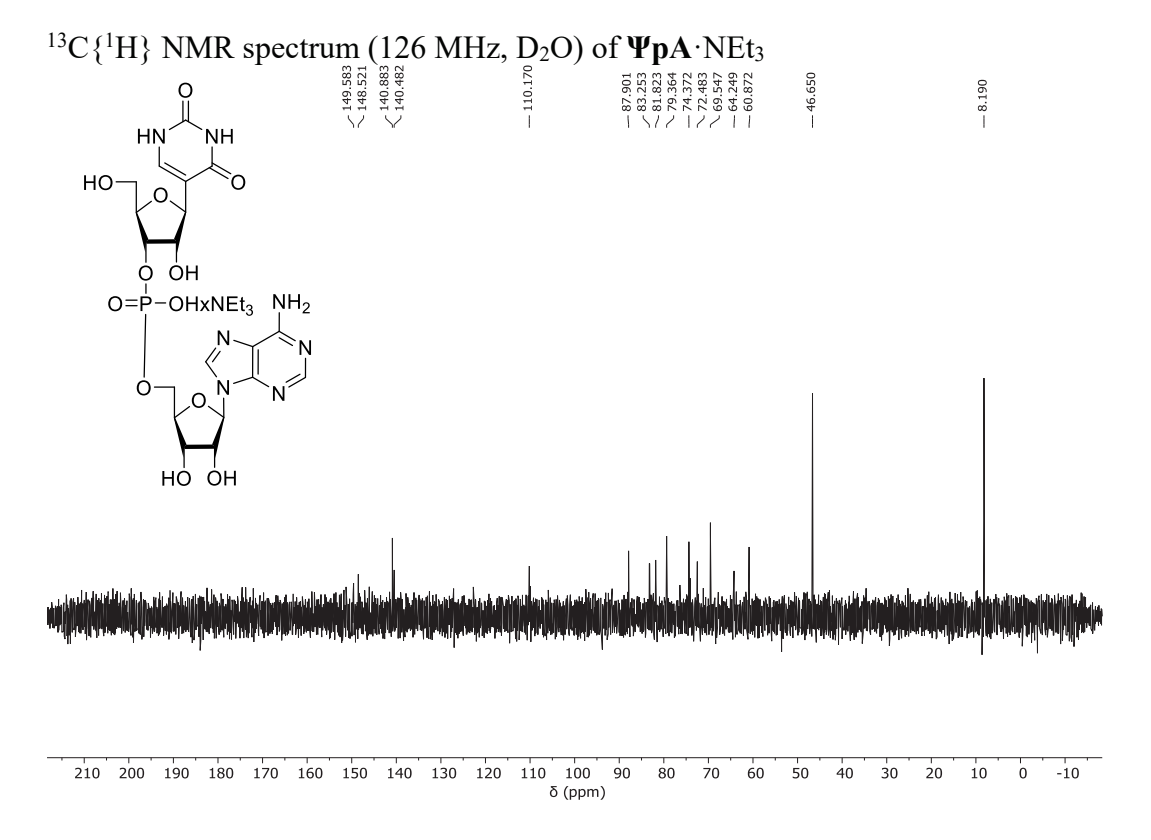


$^{31}P\{^{1}H\}$ NMR spectrum (162 MHz, D2O) of $\textbf{UpA} \cdot \text{NEt}_{3}$

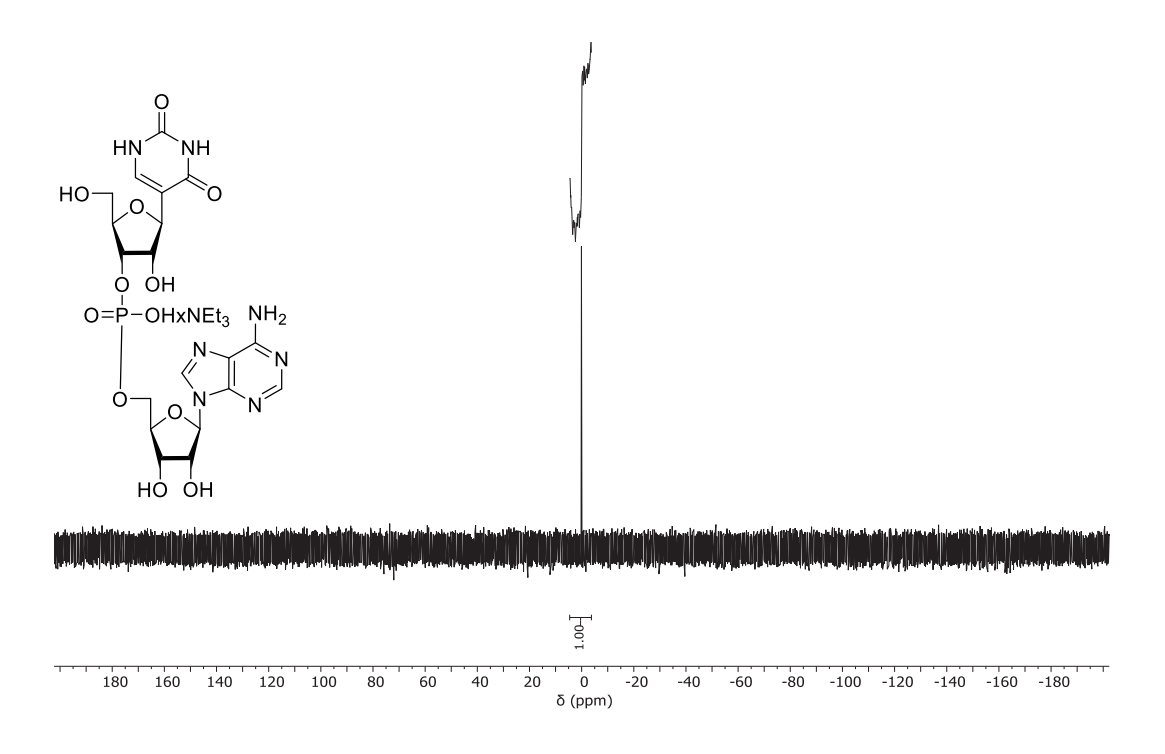


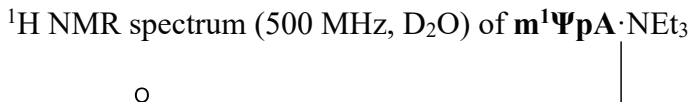


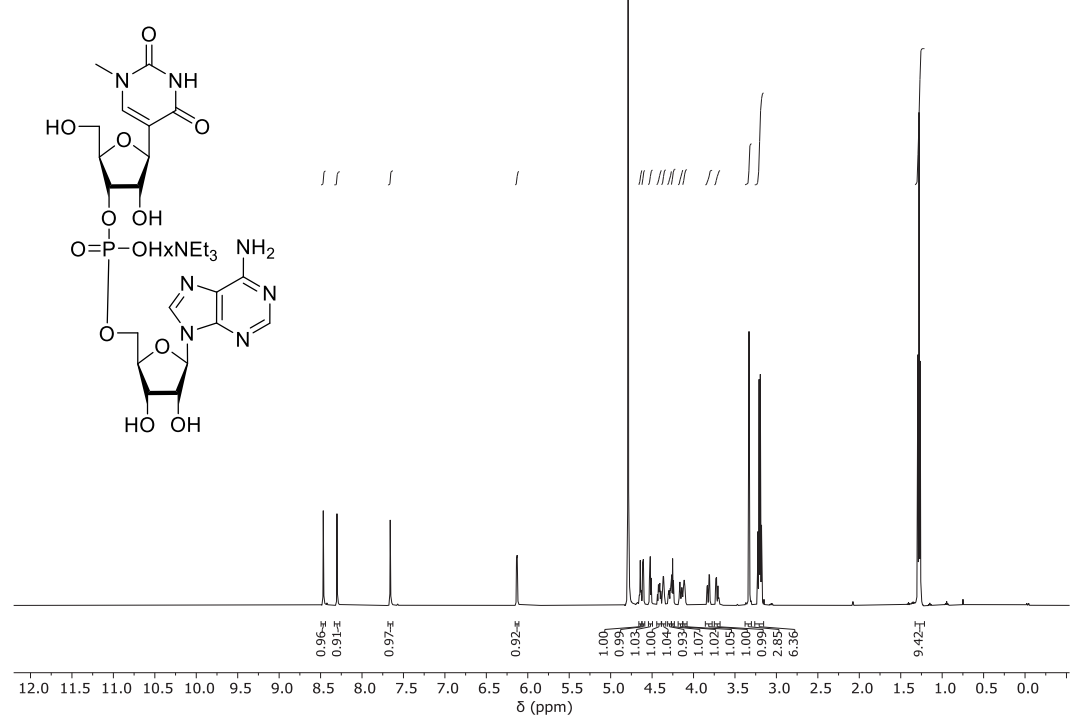


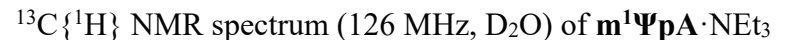


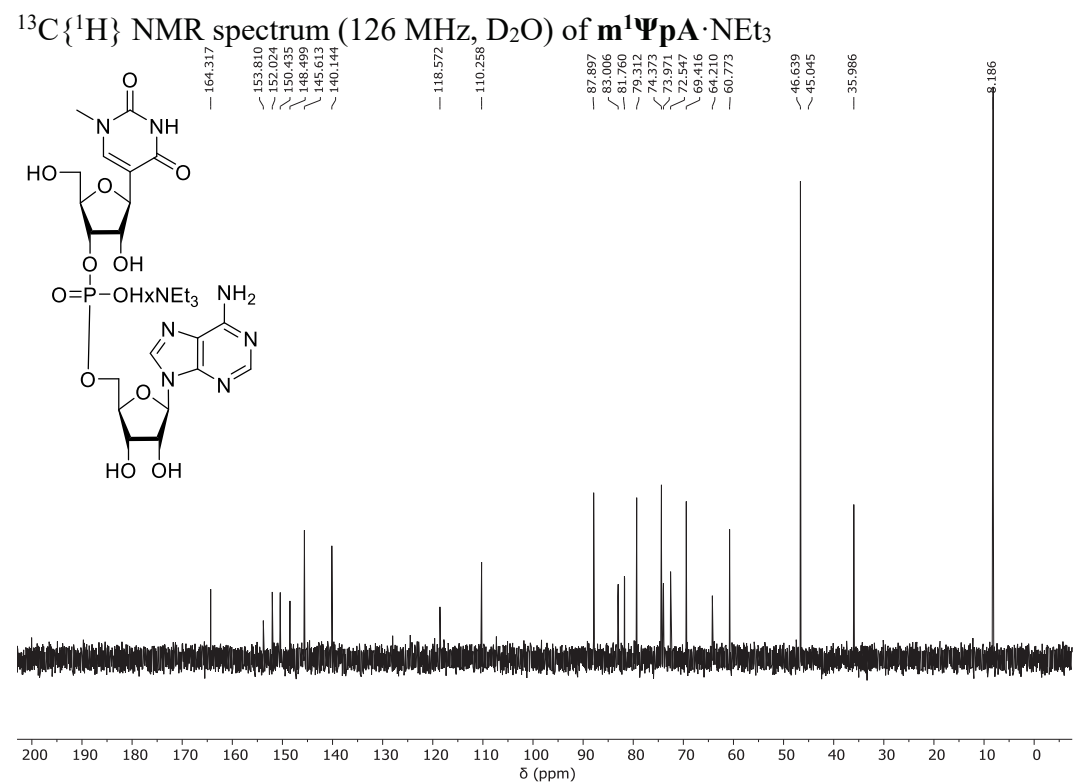
 $^{31}P\{^{1}H\}$ NMR spectrum (202 MHz, $D_{2}O)$ of $\pmb{\Psi pA\cdot NEt_{3}}$

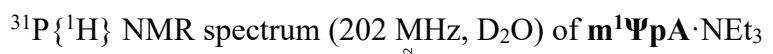


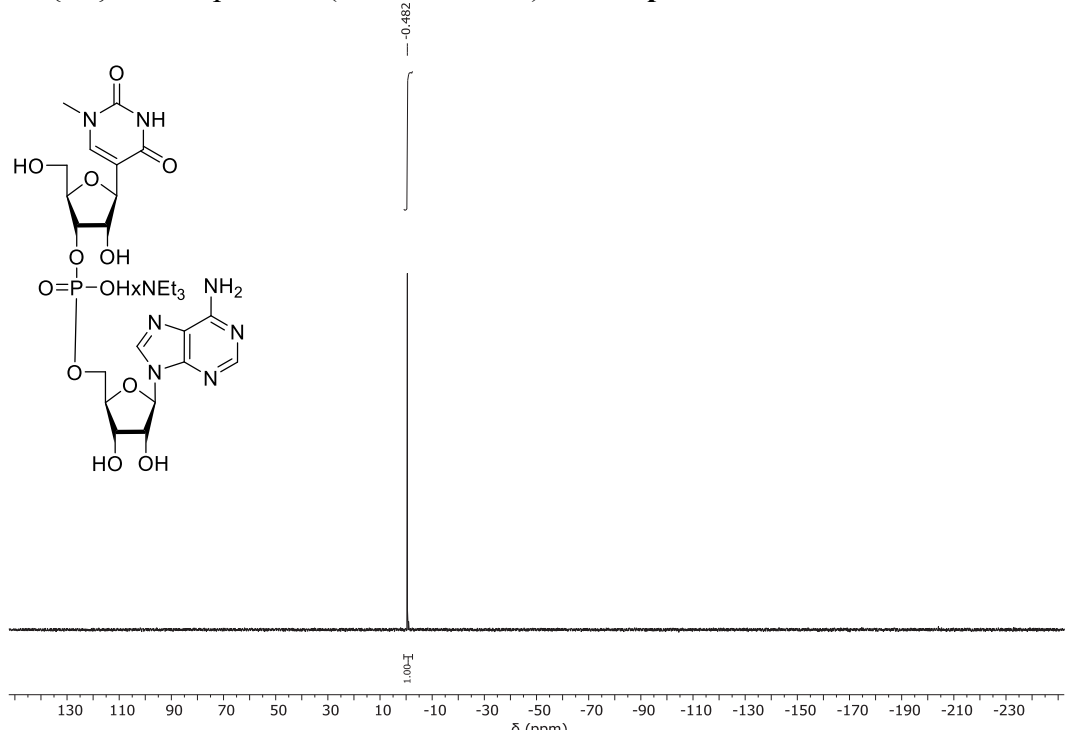












13. References

- Aureliano M, Gumerova NI, Sciortino G, Garribba E, Mclauchlan CC, Rompel A, Crans DC. 2022. Polyoxidovanadates' interactions with proteins: An overview. *Coord Chem Rev* **454**: 214344.
- Beaven GH, Holiday ER, Johnson EA. 1955. Optical properties of nucleic acids. In *The Nucleic Acids*, (ed. E Chargaff, JN Davidson), p. 493–553. Academic Press, New York, NY.
- Bisswanger H. 2014. Enzyme assays. *Perspect Sci* 1: 41–55.
- Finol E, Krul SE, Hoehn SJ, Lyu X, Crespo-Hernández CE. 2024. The mRNACalc webserver accounts for the *N*¹-methylpseudouridine hypochromicity to enable precise nucleoside-modified mRNA quantification. *Mol Ther Nucleic Acids* **35**: 102171.
- Hakimelahi GH, Proba ZA, Ogilvie KK. 1982. New catalysts and procedures for the dimethoxytritylation and selective silylation of ribonucleosides. *Can J Chem* **60**: 1106–1113.
- Hisamatsu Y, Hasada K, Amano F, Tsubota Y, Wasada-Tsutsui Y, Shirai N, Ikeda S-i, Odashima K. 2006. Highly selective recognition of adenine nucleobases by synthetic hosts with a linked five-six-five-membered triheteroaromatic structure and the application to potentiometric sensing of the adenine nucleotide. *Chem Eur J* 12: 7733–7741.
- Kelemen BR, Klink TA, Behlke MA, Eubanks SR, Leland PA, Raines RT. 1999. Hypersensitive substrate for ribonucleases. *Nucleic Acids Res* **27**: 3696–3701.
- Kotch FW, Sidorov V, Lam Y-F, Kayser KJ, Li H, Kaucher MS, Davis JT. 2003. Water-mediated association provides an ion pair receptor. *J Am Chem Soc* **125**: 15140–15150.
- Ladner JE, Wladkowski BD, Anders Svensson L, Sjolin L, Gilliland GL. 1997. X-ray structure of a ribonuclease A-uridine vanadate complex at 1.3 Å resolution. *Acta Crystallogr D Biol Crystallogr* **53**: 290–301.
- Messmore JM, Raines RT. 2000. Decavanadate inhibits catalysis by ribonuclease A. *Arch Biochem Biophys* **381**: 25–30.
- Razkin J, Nilsson H, Baltzer L. 2007. Catalysis of the cleavage of uridine 3'-2,2,2-trichloroethylphosphate by a designed helix—loop—helix motif peptide. *J Am Chem Soc* **129**: 14752–14758.
- Sayers J, Wralstad EC, Raines RT. 2021. Semisynthesis of human ribonuclease–S. *Bioconjugate Chem* 32: 82–87.
- Smith BD, Soellner MB, Raines RT. 2003. Potent inhibition of ribonuclease A by oligo(vinylsulfonic acid). *J Biol Chem* **278**: 20934–20938.
- Smith PK, Krohn RI, Hermanson GT, Mallia AK, Gartner FH, Provenzano MD, Fujimoto EK, Goeke NM, Olson BJ, Klenk DC. 1985. Measurement of protein using bicinchoninic acid. *Anal Biochem* **150**: 76–85.
- Wralstad EC, Raines RT. 2024. Sensitive detection of SARS-CoV-2 main protease 3CL^{pro} with an engineered ribonuclease zymogen. *Protein Sci* **33**: e4916.